HHS Public Access

Author manuscript

J Mech Behav Biomed Mater. Author manuscript; available in PMC 2017 September 01.

Published in final edited form as:

J Mech Behav Biomed Mater. 2016 September ; 62: 619–635. doi:10.1016/j.jmbbm.2016.05.005.

LARGE STRAIN STIMULATION PROMOTES EXTRACELLULAR MATRIX PRODUCTION AND STIFFNESS IN AN ELASTOMERIC SCAFFOLD MODEL

Antonio D'more[1,2,3,*], **Joao Soares**[4,*], **John A. Stella**[1], **Will Zhang**[4], **Nicholas J. Amoroso**[1], **John E. Mayer Jr.**[5], **William R. Wagner**[1], and **Michael S. Sacks**[4,**]

[1]Department of Bioengineering, McGowan Institute for Regenerative Medicine, University of Pittsburgh, Pittsburgh, PA USA

[2]Fondazione RiMED, Italy

[3]DICGIM, Università di Palermo, Italy

[4]Center for Cardiovascular Simulation, Institute for Computational Engineering and Sciences, Department of Biomedical Engineering, The University of Texas at Austin, Austin TX USA

[5]Department of Cardiac Surgery, Boston Children's Hospital and Harvard Medical School, Boston, MA USA

Abstract

Mechanical conditioning of engineered tissue constructs is widely recognized as one of the most relevant methods to enhance tissue accretion and microstructure, leading to improved mechanical behaviors. The understanding of the underlying mechanisms remains rather limited, restricting the development of in silico models of these phenomena, and the translation of engineered tissues into clinical application. In the present study, we examined the role of large strip-biaxial strains (up to 50%) on ECM synthesis by vascular smooth muscle cells (VSMCs) micro-integrated into electrospun polyester urethane urea (PEUU) constructs over the course of 3 weeks. Experimental results indicated that VSMC biosynthetic behavior was quite sensitive to tissue strain maximum level, and that collagen was the primary ECM component synthesized. Moreover, we found that while a 30% peak strain level achieved maximum ECM synthesis rate, further increases in strain level lead to a reduction in ECM biosynthesis. Subsequent mechanical analysis of the formed collagen fiber network was performed by removing the scaffold mechanical responses using a strain-energy based approach, showing that the de-novo collagen also demonstrated mechanical behaviors substantially better than previously obtained with small strain training and comparable to mature collagenous tissues. We conclude that the application of large deformations can play a critical role not only in the quantity of ECM synthesis (i.e. the rate of mass production), but also

**For correspondence: Michael S. Sacks, Ph.D., W. A. "Tex" Moncrief, Jr. Simulation-Based Engineering Science Chair I, 201 East 24th Street, One University Station, C0200, The University of Texas at Austin, Austin TX 78712, Tel: 512-232-7773, Fax: 512-232-7508, msacks@ices.utexas.edu.

*Equal contribution as first authors

on the modulation of the stiffness of the newly formed ECM constituents. The improved understanding of the process of growth and development of ECM in these mechano-sensitive cell-scaffold systems will lead to more rational design and manufacturing of engineered tissues operating under highly demanding mechanical environments.

Keywords

Mechanical properties; ECM (extracellular matrix); elastomeric scaffold; mechanical conditioning

1. INTRODUCTION

To date, the understanding of how various forms of biophysical stimulation promote the formation of ECM, enhance its mechanical properties, and ultimately facilitate tissue growth and development remains limited. Different forms of physical cues include ultrasound waves (Duarte 1983), electromagnetic fields (Bassett et al. 1974), or physiologic pulsatile flow patterns (Hahn et al. 2007). Collectively, these have led to mechanical conditioning as a widely recognized a highly relevant factor influencing tissue accretion, micro-structure, all affecting the bulk mechanical response (de Jonge et al. 2013a; Engelmayr et al. 2005; Engelmayr and Sacks 2008; Engelmayr et al. 2006; Hasaneen et al. 2005; Haseneen et al. 2003; Huey and Athanasiou 2011; Kim et al. 1999; Merryman et al. 2007; Nerurkar et al. 2011c; Rubbens et al. 2009; Syedain and Tranquillo 2009; von Offenberg Sweeney et al. 2004).

However, the complexity of the underlying strain transfer mechanisms from the tissue to cellular levels remains poorly understood. Initial studies have focused on the macroscopic scale (>1 mm) and aimed to describe the effects of stimulating strains on cell-seeded engineered tissue constructs (Mol et al. 2005; Seliktar et al. 2000; Stella et al. 2010; Syedain and Tranquillo 2009; Syedain et al. 2008). In an effort to elucidate the chain of events involved in transferring strain from the organ level down to tissue and cellular levels, a second generation of in vitro studies shifted their focus towards the effects of mechanical strain at the mesoscopic level (>10 μm and < 1mm) (de Jonge et al. 2013a; Engelmayr et al. 2005; Engelmayr and Sacks 2008; Lee et al. 2005; Stella et al. 2010). Focusing on the biochemical pathways of mechanical transduction at the meso-scale, Baker et al. proved the correlation between mechanical forces, transforming growth factor β (TGF-β) signaling, and the subsequent hypertrophy of vascular cells (Baker et al. 2008). In parallel, multi-scale models (Aghvami et al. 2013; Breuls et al. 2002; Stylianopoulos and Barocas 2007b) have grown in sophistication bridging the organ-tissue-cellular scales and providing powerful tools to predict the deformation of fibers and cells resulting from global mechanical strains (Sander et al. 2009). Specifically, structural deterministic approaches have the ability to model idealized (Stylianopoulos and Barocas 2007a) or realistic (D'Amore et al. 2014) ECM structural components and to relate these to the macroscopic forces acting on the tissue construct (e.g. (Soares and Sacks 2015)).

Overall, there is a trend from empirically-based trial-and-error prototypes towards a rational approach based on engineering principles and critical reasoning with idealized in vitro

models at the tissue/cellular level. Since these in vitro models cannot fully mimic the in vivo milieu, they are more suitable to understand the mechanisms of ECM development resulting from their high level of controllability and reproducibility. One can describe these goals generally as: (i) means to improve the general understanding of the interplay between mechanics and cellular biosynthesis, and (ii) achieve the goal of obtaining functional and designed engineered constructs at the organ level. Yet, despite these efforts, developing a thorough understanding of the underlying structural and mechanical factors responsible for the formation and maturation of functional ECM structures remains elusive (Amoroso et al. 2012; Amoroso et al. 2011; Courtney et al. 2006; Soares and Sacks 2015). Several limitations affect the capacity of existing in silico and in vitro models and hamper critical development of the in vivo objective. The most relevant limiting factors include: (i) the relatively limited strain range imposed by current bioreactor and scaffolds technologies; (ii) the complexity of experimentally accessible quantitative metrics for scaffold-cell mechanical interactions (e.g. nuclear or cell aspect ratio, single ECM fibers stretch, and de novo ECM mass in vivo); and (iii) the lack of experimental and numerical techniques able to de-couple intrinsic scaffold mechanical behaviors from the newly formed ECM mechanical behaviors.

In the current study, we sought to begin to address these limitations by investigating the role of large strains on seeded elastomeric scaffolds. We hypothesized optimal dynamic conditioning regimes with large deformations (within the physiologic ranges of up to 50% strain at 1 Hz) exist, and that these can be exploited to augment ECM production and improve matrix mechanical behavior, i.e. large deformation stimuli improves produced ECM quantity and quality. By utilizing cell integrated (Courtney et al. 2006) electrospun scaffolds (Guan et al. 2004; Stankus et al. 2004) we were able to investigate the effect of tissue level finite deformation on ECM synthesis. VSMCs micro-integrated into electrospun PEUU scaffolds were selected as a suitable fabrication technique for cell seeding (Courtney et al. 2006), to be subjected to large strains, and to possess elastic moduli of interest for soft tissue engineering applications (D'Amore et al. 2014), and most importantly, are a mechano-sensitive cell-scaffold system (Stella et al. 2008). Mechanical evaluation experimental evaluation coupled to a ECM structural modeling approach were adopted to predict and de-couple scaffold and de novo ECM mechanics.

2 – Methods

2.1-Construct fabrication and cell source

Biodegradable, elastomeric tissue constructs micro-integrated with rat VSMCs were manufactured by concurrent cell electrospraying and polymer electrospinning as previously described (Guan et al. 2004; Stankus et al. 2006). The electrospinning process produces continuous fiber scaffolds exhibiting tunable mechanical properties while providing a suitable environment for cell proliferation and growth. Control of fiber alignment is obtained by variations of the rotational velocity of the mandrel, resulting in scaffolds with a high degree of fiber alignment and preferred and cross-preferred fiber directions.

Cellular micro-integration into the polymeric scaffold was obtained with concurrent electrospraying. VSMCs were isolated from Lewis rat aortas (conducted at University of Pittsburgh in accordance with Institutional Animal Care and Use Committee guidelines), and

were expanded on tissue culture polystyrene flasks using Dulbecco's modified Eagle medium (DMEM) (Lonza) with 10% fetal bovine serum and 1% penicillin-streptomycin. Electrospraying of rat VSMCs during electrospinning was accomplished by feeding 1×10^7 cells/mL into a sterilized capillary charged at +7 kV and located 4 cm from the target mandrel (19.05 mm diameter) concurrent with PEUU/1,1,1,3,3,3-hexafluoroisopropanol solution (12-wt%, Oakwood Products) electrospinning from a capillary charged at +12 kV and located 20 cm from the target mandrel (Figure 1a). Cell concentrations in the electrospray solution were determined using a BRIGHT-LINE hemocytometer (Hausser Scientific). The collecting mandrel was charged at −4 kV and was rotated at 150 rpm while translating 8 cm along the z-axis at 0.15 cm/s. After 30 min of electrospinning and electrospraying, the microintegrated tube was cut and removed from the mandrel and placed into static culture media (DMEM, 10% fetal bovine serum, 2% anti-anti, 1% HEPES) for 24–48 h prior to mechanical conditioning. Some degree of fiber alignment in the PEUU is induced by the combination of the stage translation speed and the mandrel length to diameter ratio, providing more opportunity for fibers to deposit parallel to the mandrel axis (Stankus et al. 2006). Thus, the longitudinal mandrel direction is referred to as the preferred fiber direction (PD) while the orthogonal or circumferential direction is the cross preferred direction (XD) (Figure 1b). The construct was cut in the circumferential direction at several points such that approximately four individual ring specimens (Figure 1c) measuring 10 mm in width were obtained. Specimen length and thickness was measured by five measurements/sample performed with a micrometer.

2.2 - Stretch bioreactor study and conditioning regimes

The bioreactor used in this study was similar to that previously presented by Merryman et al. (Figure 2) (Merryman et al. 2007). Modifications were made to update the system enabling improved deformation control. Motion control was conducted through custom Labview software (National Instruments, NI) with an individual stepper motor controller (NI PCI-7334) and integrated stepper driver and power unit (NI MID-7604). The computer controlled stepper motor (Haydon Kerk Motion Solutions) drives a linear actuator passing through the chamber wall. The actuating arm has two orthogonal crossbars with exiting holes into which stainless steel pins are inserted. These pins align directly across from the stationary pins to apply uni-directional tension to up to 8 specimens simultaneously. The 8 separate well arrangement was chosen to limit the risk of cross contamination. The microintegrated VSMC-PEUU construct rings were inserted into the stretch bioreactor (Figure 2) by sliding the pins of the actuating and stationary posts through the ring annulus (Merryman et al. 2007). In each well, 7 mL of complete media was added and changed every 24 hours. The entire device, including lids, pins, and screws, was cold gas sterilized with ethylene oxide prior to specimen loading.

Native soft tissues experience large deformations in vivo, thus and the role of large strains is of paramount relevance in engineered tissue design. Both simulations and experimental findings have demonstrated that elastomeric scaffolds and bioprosthetic heart valve leaflets experience large strains in the range of 10% to 30%. More specifically, physiologic strain levels with peak values of ~30% were predicted by Fan et al. (Fan et al. 2013a) via finite element simulations of electrospun polyester-urethane-urea heart valve leaflets in the

pulmonary position (Fig. 8b). Similarly, Aggarwal et al. (Aggarwal and Sacks 2015a) (Aggarwal and Sacks 2015b) applied an inverse modeling approach to capture experimentally derived deformations on the Carpentier-Edwards Perimount Mitral Valve, a commercially available bioprosthetic valve. In this study a Green-Lagrange strain range of 5%–12% corresponded to a physiologically relevant 2nd Piola Kirchhoff stress of 500kPa (Fig. 6 a). Finally, Aggarwal et al. (Aggarwal et al. 2013) described methods and protocol to derive patient specific valve leaflet deformation maps. Results showed that human aortic valve leaflet is characterized in vivo by a Jacobian of about 1.2 (invariant of the Green's strain tensor representing the change in area upon deformation) (Fig. 4 b).

Hence we utilized strain range of up to 50% that encompasses these values. The biosynthetic response of VSMC-PEUU constructs was investigated at 1 Hz cycle for three culture durations of 7, 14, 21 day time points and for 3 cyclic strain levels within normal heart valve physiology: low (15%), intermediate (30%), and high (50%). For comparison purposes, 0 day and static cultured groups were also carried out as well as control groups comprised of acellular electrospun PEUU. The adoption of control groups establishes a baseline to study the specific effects of strain on ECM production (Merryman et al. 2007). Upon completion of the mechanical training protocol, specimen rings were removed from the bioreactor, and specimen length, width, and thickness were measured for comparison with specimen dimensions prior to mechanical training.

2.3 – Biochemical assays and histology

After dimensional changes were recorded, construct rings were dissected into segments for biochemical analysis. Full width cuts were carried out at both locations that came in contact with the loading pins resulting in two segments. Due to compressive forces experienced at the loading pin regions, the specimen consistently exhibited a compressed morphology and this region of the construct was trimmed and discarded from further use. One segment was dedicated to collagen assays while the other segment was again bisected in the PD such that a small 2 mm segment was obtained and immediately placed in 10% buffered formalin for histological analysis. The remaining segments were then bisected in the XD with a portion of each being used for GAG and DNA quantification assays respectively.

DNA was quantified by a technique adapted from Kim et al (Kim et al. 1988). For each assay, samples were lightly patted dry with paper towel to remove excess fluid and weighed prior to extraction. Each sample was placed in a microcentrifuge tube and extracted in 1 ml papain solution for 10 h in a 60 °C water bath. The papain solution was made immediately prior to use by adding L-cysteine dihydrochloride (Sigma) to a phosphate buffered EDTA solution to a concentration of 10 mM, clarifying the solution using a syringe-driven filter (0.2 μm Millex®-LG PTFE membrane; Millipore), and adding papain (minimum 10 units/mg (P4762); Sigma) to a concentration of 0.125 mg/mL. The PBE solution was made beforehand by adding sodium phosphate dibasic (Sigma) and ethylenediaminetetraacetic acid (EDTA; Sigma) to deionized water at concentrations of 100 mM and 10 mM, respectively. The PBE solution was balanced to pH 6.5 with 0.5 N hydrochloric acid (Sigma) and sterile filtered. The extracts were assayed using the PicoGreen dsDNA quantitation kit

(Molecular Probes) per the manufacturer's instructions and using the blue channel of a TBS-380 Mini-Fluorometer (Turner Biosystems).

Collagen and sulfated glycosaminoglycans (sGAG) were assayed by techniques adapted from Brown et al. (Brown et al. 2000). For each assay, samples were lightly patted dry with paper towel to remove excess fluid and weighed prior to extraction. Total collagen was extracted from samples using a solution of 0.5 M acetic acid (Sigma) and pepsin (1 mg/mL Pepsin A (P-7000); Sigma). Each sample was placed in a microcentrifuge tube and incubated in 1 mL of extraction solution overnight (~ 16 h) on a rocker (Orbitron Rotator I™; Boekel Scientific) in a refrigerator at 2–8°C. Proteoglycans and S-GAG were extracted using a solution of 4 M guanidine-HCl (Sigma) and 0.5 M sodium acetate (Sigma). To minimize proteolysis during the extraction, 100 μL of protease inhibitor cocktail stock solution was added to each extraction solution. The stock solution was prepared according to the manufacturer's recommendations by dissolving one Complete Mini Protease Inhibitor Tablet™ (Roche Diagnostics) in 1.5 mL of deionized water. Each sample was incubated in 1 mL of extraction solution overnight on a rocker table (Boekel Scientific) in a refrigerator at 2–8°C. Following the extraction steps, the collagen and S-GAG extracts were assayed according to the guidelines provided with the Sircol™ and Blyscan™ assay kits, respectively (Biocolor) using a Genesys 20 spectrophotometer (Thermo Spectronic).

Histological evaluations were carried out on dedicated specimen segments via paraffin embedding. Serial sections (6 μm) were stained with hematoxylin and eosin (H&E) for morphology, and with picrosirius red (PSR), a collagen protein specific stain. An image analysis based protocol was implemented to analyze digitized histological sections to determine ECM area fraction. Representative full thickness images stained with PSR and H&E were chosen from the 14 and 21-day time points respectively. The color images were converted to greyscale for each channel. The biological phase was most apparent in the green channel for both stain types. A threshold was applied to: (i) segment the entire area encompassed by the construct, and (ii) segment only the ECM portion of the section. Both measurements were necessary to accurately calculate the matrix area fraction while accounting for regions of the image that did not contain ECM or polymer (i.e. voids within the specimen and areas outside). The collagen area fraction was determined as the ratio of the collagen area to the total area. The analysis was carried out for 5 samples.

We note that in pilot studies mature-appearing collagen fibers were the only ECM structural protein produced (no elastin was observed) so that in all subsequent analysis we refer to collagen when discussing ECM mechanical behaviors. More specifically, our preliminary runs consisted of VSMCs-PEUU samples conditioned for 21 day at 30% strain and 1 [Hz] frequency (n=4). Verhoeff-Van Gieson (VVG), Picrosirius red and H&E stains were utilized to identify elastin, collagen and ECM/polymer components respectively. While collagen fibers were identified by Picrosirius and H&E staining confirming the presence and elaboration of de novo collagen, VVG and H&E staining comparison showed no trace of elastin with VVG positive areas being co-localized with areas occupied by the polymer fibers in the H&E processed sections (Supplemental Fig. 1).

2.4 – Mechanical evaluation

Testing specimens of microintegrated VSMCs-PEUU engineered tissue constructs mechanically conditioned for 21 day at 30% were cut to square dimensions 10 mm × 10 mm with specimen edges aligned to the longitudinal (x_1 – PD) and (x_2 – XD) directions of the rings. Thin sections of polypropylene mono-filament suture were cut to form four small fiducial markers in the central 3 × 3 mm region of the specimen. Engineered tissue construct test specimens (n = 5) were prepared for planar biaxial mechanical testing under stress control, and the four sides of each specimen were tethered using nylon suture and small stainless steel hooks (Zhang et al. in press). The test specimen was then mounted onto a custom made planar biaxial testing device. Each side of the square test specimen was connected to the motor carriages via sutures to apply four point loads. The load on each axis was constantly monitored using force transducers (with a signal conditioner) and the applied load was controlled by adjusting the stepper motors using custom software and a data acquisition board installed on a PC. Testing was performed at room temperature, in deionized water, under stress control, and starting from a preload of 0.5 g. Standard methods were used to determine the in-plane strain and Cauchy stress tensor T and first Piola-Kirchhoff stress tensor P assuming tissue incompressibility (Zhang et al. 2015).

Engineered-tissue testing specimens (n = 5) were preconditioned for 10 cycles under equibiaxial stress, up to the determined maximum testing stress of 300 kPa. In all analyses, the post-preconditioned 0.5 g tare configuration was used as the reference state. The testing protocol consisted of axial stress ratio controlled paths (P_{11}:P_{22} = 30:300, 150:300, 225:300, 300:300, 300:225, 300:150, 300:30) using a half cycle time of 15 s to quantify the quasi-static response. These ratios were chosen to cover a wide range of stress states. Total testing time was approximately 2 h per specimen.

2.5 – Collagen degradation protocol and subsequent biaxial testing

Probing the mechanical contribution of each phase of the construct (i.e. polymer or matrix) necessitated the ability to isolate an individual phase for mechanical characterization. Since the polymer phase comprised the majority of the construct in terms of volume fraction and stress generation, it was most practical to isolate this phase by removing the biological portion of the construct. This was accomplished by placing the specimen in 0.25% Trypsin EDTA (Invitrogen) for 24 h at 37 °C. Validation of the success of the degradation protocol was carried out by staining adjacent sections before and after degradation with H&E for visual comparison. The same biaxial testing protocol outlined above was again used after degradation to quantify the PEUU scaffold mechanical behavior. After matrix degradation, construct compliance was observed to increase significantly, requiring a subsequent reduction of the peak stress at run time to 200 kPa. This approach enables the direct comparison of the biaxial mechanical response of the total construct with its subsequent degraded mechanical behavior. Lastly, in order to verify that the degradation protocol did not affect scaffold mechanical properties per se, the mechanical response of 6 acellular scaffolds was compared before and after degradation with the same biaxial testing protocol.

2.6 – Modeling the de novo collagen mechanical behavior

The resulting stored energy density can be calculated for each protocol based on the stress and strain relationship measured along the loading paths of the biaxial testing protocol. Assuming that zero energy is stored at the initial tare configuration (stress free reference configuration), the stored energy density ψ can be computed by:

$$\psi = \int S_{11} dE_{11} + \int S_{22} dE_{22} + \int S_{12} dE_{12}, \quad (1)$$

where S_{ij} are the components of the second Piola-Kirchhoff stress and E_{ij} are the components of the Green strain. Values of stress and strain are experimentally derived during the biaxial testing protocol. Due to the on-material axis configuration of the biaxial experiment, the contribution of the shear component $S_{12} \approx 0$.

The testing protocol was comprised of seven stress-controlled loading paths that defined consistently convex surfaces in $\psi(E_{11},E_{22})$ space. The resulting $\psi(E_{11},E_{22})$surface was fit to a biquintic finite element surface (Fata et al. 2014). The methodology described allows for direct subtraction of fitted strain energy-surfaces for each sample individually before ($\psi_{construct}$) and after trypsin treatment (ψ_{PEUU}) as follows. Assuming that no stored energy is associated with collagen-scaffold mechanical interactions, the stored energy density surface of the collagen phase can be calculated using

$$\psi_{collagen} = \psi_{PEUU+collagen} - \psi_{PEUU}. \quad (2)$$

In order to obtain further insight on the structural and mechanical behaviors of the de-novo synthesized collagen, the collagen mechanical data was fit to the following structural constitutive model (Fan and Sacks 2014; Zhang et al. in press),

$$\mathbf{S}_c = \phi_c \eta_c \int_{-\pi/2}^{\pi/2} \Gamma(\theta) \left[\int_0^{E_{ens}} D(x) \frac{E_{ens} - x}{(1+2x)^2} dx \right] (\mathbf{N} \otimes \mathbf{N}) d\theta + (1-\phi_c)\mu_m (\mathbf{I} - C_{33}\mathbf{C}^{-1}). \quad (3)$$

Here φ_c is the mass fraction of the collagen fibers, η_c is the stiffness of the collagen fibers, $\Gamma(\theta)$ is the collagen fiber orientation distribution defined on $\theta \in [-\pi/2,\pi/2]$, $D(x)$ is the recruitment distribution function defined on $x \in (0,E_{ens})$ with the upper bound of integration being the fiber ensemble strain, and μ_m is the matrix stiffness. The fiber orientation distribution $\Gamma(\theta)$ is expressed as a linear combination of a Gaussian distribution and uniform distribution:

$$\Gamma(\theta) = d \left[\frac{\exp\left(-\frac{(\mu-\theta)^2}{2\sigma^2}\right)}{\operatorname{erf}\left(\frac{\pi}{2\sqrt{2}\sigma}\sqrt{2\sigma}\right)} \right] + \frac{1-d}{\pi}, \quad (4)$$

where d represents the ratio of aligned fibers (first term) to the randomly oriented fibers, μ is the average alignment orientation, and σ denotes the standard deviation of the Gaussian distribution function and represents the fiber splay. For curve-fitting, $d = 1$ was considered while μ and σ were allowed to vary. The recruitment function is represented as a Beta distribution defined as:

$$D(x)=\begin{cases} \frac{x^{\alpha-1}(1-x)^{\beta-1}}{B(\alpha,\beta)(E_{ub}-E_{lb})}, & \text{for } x\in[0,1], x=(E_{ens}-E_{lb})/(E_{ub}-E_{lb}) \\ 0, \quad \text{otherwise} \end{cases} \tag{5}$$

where α and β are shape factors, related to mean μ_R and standard deviation σ_R of the Beta distribution B(α,β) defined by

$$\overline{\mu}_R=(\mu_R-E_{lb})/(E_{ub}-E_{lb}), \quad \overline{\sigma}_R=\sigma_R/(E_{ub}-E_{lb}) \tag{6}$$

$$\alpha=\frac{\overline{\mu}_R{}^2-\overline{\mu}_R{}^3+\overline{\sigma}_R{}^2\overline{\mu}_R}{\overline{\sigma}_R{}^2}, \quad \beta=\alpha\frac{1-\overline{\mu}_R}{\overline{\mu}_R}$$

As in our previous studies (Fata et al. 2014), from the interpolated equibiaxial strain response ($E_{11} = E_{22}$) the ECM collagen fiber ensemble response were derived using

$$S_{ens}=S_{11}+S_{22} \text{ and } E_{ens}=E_{11}=E_{22} \tag{7}$$

Lower and upper bounds of the fiber-ensemble strain response were imposed at $E_{lb} = 0$ and E_{ub} determined from the S_{ens} vs. E_{ens} diagrams. Subsequently, parameters [η,μ,σ,μ_R,σ_R] are determined from the best fit minimizing the discrepancy between model-predicted and experimentally-measured stored energy density surfaces. The minimization procedure was applied individually to each sample resulting in a stored energy density function $\psi_{collagen} = \psi_{collagen}(E_{11},E_{22})$ and a set of structural model parameters [η,μ,σ,μ_R,σ_R] characterizing each individual sample response, which were then combined as mean ± standard deviation. Subsequently, samples were coalesced into an average stored energy density surface representing average response of the de novo collagen of all samples (n = 5). The same methodology was adopted to obtain the model parameters describing the average response. Lastly, experimental results obtained by Sacks and Chuong (Sacks and Chuong 1998) for native bovine pericardium (BP) were included for comparison to mature dense collagenous membrane tissues

2.7 – Statistical analysis

Statistical analysis was performed using Sigma plot (Systat Software Inc., Chicago, IL, USA). One-way analysis of variance (ANOVA) followed by Turkey multiple comparison test was utilized for comparison of multiple groups. Student's T-test was utilized for

comparison of two groups. Results (n>5) are presented as mean ± standard deviation and differences were considered to be statistically significant at $p<0.05$.

3 – RESULTS

3.1 – Conformational effects of mechanical training

Mechanical training induced dimensional changes in the engineered tissue constructs and acellular scaffolds. Measurable changes occurred in elongation and thickness, whereas changes in width were not significant. The duration of the mechanical training and magnitude of the imposed cyclic deformation were significant contributors to specimen elongation (Figure 3a). Acellular scaffolds exposed to 30% strain cyclic deformation for 21 day exhibited significantly more ($p<0.05$) elongation (17.8%) than those that were micro-integrated, that reported from 6% to 12.4% elongation. Regardless of the time-point elongation was significantly impacted by the strain magnitude. Matrix deposition had a profound effect on construct thickness, micro-integrated constructs at 21 day of 30% cyclic strain had an average thickness increase of 18.8 ± 3.1% while acellular scaffolds subjected to similar conditions exhibited a thickness decrease of 25.0 ± 7.6%. Dimensional changes were combined into volumetric changes (Figure 3b). No observable change in volume was observed in any specimens at 7 day. At 14 day, 30% and 50% strain groups exhibited substantial increase in total volume with the 30% being significantly larger than the other groups. Based on this result, as well as on the significantly higher collagen deposition reported in the 30% strain group (Figure 5b), cellular synthetic behavior and volumetric changes were further studied at a later time point of 21 days, and the substantial increase in volume when compared with the acellular control group was more pronounced (Figure 3b). This change in volume was due to increases both in elongation and thickness, while for the acellular control group the increase in elongation was compensated by a decrease in thickness. Integrity of constructs subjected to 50% cyclic strain was low, possibly due to harsh mechanical stimuli and non-sufficient ECM production, causing delamination non-reliable measures of thickness in this group.

3.2 - Collagen synthesis analysis with biochemical composition and histological assessment

Histological staining with H&E for general morphological assessment (Figure 4a) and picrosirius red (PSR) (Figure 4b) indicated clear modulation of the VSMC activity in terms of ECM synthesis due to mechanical conditioning. VSMCs were distributed well throughout the construct thickness at the time of manufacturing. After the application of 30% cyclic strain for 14 day, collagen and cell rich regions were formed (denoted by dark bans through the construct), whereas static and 15% strain groups showed little discernible difference from day 0. Cellular viability was good, with lamellar cellularized regions were formed. The highest collagen deposition for the 30% strain group quantified in Figure 5 b and observed in Figure 4 by H&E and PSR stain, created a more mechanically robust engineered constructs that were less prone to delaminate during the samples sectioning process required by the histological assessment.

In order to account for inter-sample variability due to variations in cellular density, collagen protein and sGAG quantity were normalized by DNA content on a wet weight basis. Biochemical assay results corroborated histological observations. At both 7 and 14 day, regardless of strain levels, all the conditioned groups experience a significantly larger sGAG deposition when compared with the day zero or the static groups (Figure 5a). However, sGAG synthesis seemed to be indifferent to strain level with non-significant differences among all the constructs subjected to dynamic training.

Significantly improved collagen synthesis was observed in specimens exposed to 30% strain when compared to all the other groups (day 0, static, 15% and 50% strain) at both 7 and 14 day. In contrast, specimens subjected to 15% at day 7 and 14 showed non-significant increase over static and day 0 specimens (Figure 5b). Finally the 50% strain group produced a significantly higher amount of collagen at 14 day when compared to the day 0, static and 15% group, but significantly lower when compared to 30% strain group, yet differences at day 7 were not significant.

The collagen area fraction determination was performed from PSR and H&E stained histological sections. Sections stained with PSR at 14 day of 30% cyclic strain conditioning showed a 5:1 ratio of PEUU to collagen, while sections stained with H&E at 21 day of the same regimen suggest 4.2:1 ratio (Table 1). The method was consistent between both straining protocols and among all 5 samples tested.

3.3 – Trypsin degradation

The trypsin degradation protocol removed the vast majority of biological components after 24 h as was confirmed visually by histological evaluation of adjacent specimen segments from the 21 day 30% cyclic strain conditioning group. Comparison of intact and degraded H&E stained construct segments clearly showed collagen removal (Figure 6). PEUU remained unstained and provided minimal contrast under bright field microscopy, where images have been inverted for improved visualization (bright green – collagen; gray – PEUU). Furthermore, to ensure that the degradation protocol did not adversely affect polymer structure and mechanical behavior, mechanical validation was carried out on five acellular specimens. Biaxial testing results showed that there was no discernable change in the mechanical response due to the enzymatic degradation protocol, with responses remarkably consistent before and after degradation indicating a high level of repeatability (Figure 7a). More specifically, interpolated values at the equi-biaxial strain path exhibited similar responses (Figure 7b). A consistent mechanical behavior was observed across all samples (Figure 7c) with a relative areal difference (before and after degradation) of the stress vs. equi-biaxial strain curves in the PD and XD directions being under 7.5%.

3.4 – Mechanical response of the de novo collagen

Systematic mechanical evaluation of constructs before and after degradation on a per specimen basis showed consistent compliance increases and allowed the determination of the mechanical contribution of the de novo collagen (Figure 8). Calculation of stored energy density at each experimental point (computed with Equation (1) and shown as dots in Figure 8a) allowed the determination of stored energy density surfaces (surfaces in Figure 8a.

Stored energy density surfaces were consistently convex and monotonically increasing, and revealed marked anisotropy characteristic of materials with preferred fiber direction.

Stored energy density in the equi-biaxial strain path was obtained with ψ-surface interpolation along the $E_{11} = E_{22}$ line (Figure 8b). Similarly, membrane tensions t_{11} and t_{22} along the equi-biaxial path were determined by interpolation of surfaces (Figure 8c), showed construct anisotropy, with stiffer response along the polymer fiber preferred direction. Subtraction of stored energy density surfaces before and after degradation provided the stored energy density associated with the collagen phase (obtained with Equation (2) and shown as green surface in Figure 8a,). The subtraction was strictly carried out in the common strain range of both ψ-surfaces. Membrane tensions response of the collagen component determined through the directional derivative of $\psi_{collagen}$ (with $t_{ij} = hP_{ij}$, $\mathbf{S}_c = \partial\psi_c/\partial\mathbf{E}_c$, and $\mathbf{P} = \mathbf{FS}$) demonstrated both the de novo collagen mechanical nonlinearity and anisotropy. The approximately exponential behavior that characterizes connective tissue was mildly present and different (Figure 8c). Lastly, the collagen fiber ensemble stress $\mathbf{S}_c$ vs. ensemble strain $\mathbf{E}_c$ (Eqn. 3) allowed the determination of the upper bound for collagen fiber recruitment $E_{ub} \approx 0.09$ as the strain at which $d^2S_{ens}/dE_{ens}^2 \approx 0$ (Figure 8d and 8e). Sample variability was minimal showing not only similar $\psi_{collagen}$-surfaces, but also consistent equibiaxial strain responses (Figure 9). Therefore, a representative stored energy function surface of the de novo ECM $\psi^{\text{avg}}_{\text{collagen}}$ can be derived by fitting lattice points (11×11) of each sample into a representative surface. The stored energy density of de novo engineered tissue compared favorably with BP at lower strains, however failed to carry higher stresses with comparable deformations of BP (Figure 9). Regardless, the substantial improvement over the stiffness of the ECM obtained by Englemayr et al. under small strain condition with flexure of VSMC-seeded needled-non-wovens is remarkable. For reference, an incompressible isotropic neo-Hookean model was assumed and $W^{SS}_{ECM} = E^{SS} w_{ECM} (I_1 - 3)/6$ where E_{SS} = 0.0904 kPa / (μg/g ww) and w_{ECM} = 893 μg/g *ww* (Engelmayr et al. 2005; Engelmayr and Sacks 2008).

3.5 – Modeling the mechanical response of the de novo collagen

The structural model predicted collagen fiber stiffness of 9.94 MPa, which corresponded to about half of 21 MPa of BP (Table 2). Comparable fiber orientation distributions were observed with splays of about 35 degrees; however, fiber recruitment occurred at minimal or at zero strain (about 8% strain in BP). Lack of undulation and mild anisotropy indicated immature micro-structural organization and maturation of highly specific dense connective tissues. Individual curve-fitting of each sample stored energy density surfaces $\psi_{collagen}$ resulted in consistent sets of model parameters (n = 3), whose average and standard deviations are comparable with the representative average stored energy density surface $\psi^{\text{avg}}_{\text{collagen}}$.

4 – DISCUSSION

4.1 – Key findings

This study is the first known to the authors to quantify the effects of large deformations on ECM synthesis and mechanical properties in elastomeric scaffolds. A novel analysis framework was presented to de-couple scaffolds from de novo ECM mechanics and to predict de novo ECM biaxial response and anisotropy. Overall results indicate that VSMC biosynthetic behavior is indeed a function of global strain with markedly improved soluble collagen synthesis in specimens exposed to 30% cyclic strain. The elastomeric nature of electrospun PEUU is conducive to the synthesis of critical structural matrix proteins, and from this perspective the scaffold system is a valid candidate for soft tissue engineering applications characterized by highly demanding mechanical environments. Sulfated glycosaminoglycan production (Figure 5a) appeared to be driven primarily by the application of cyclic deformation regardless of the strain levels as seen by the response for all dynamically conditioned specimens (Figure 5b). For this reason no further analysis was conducted on sGAG deposition at day 21 and we expected that no substantial differences among training levels will develop from 7 and 14 to 21 days.

In quantifying the effects of controlled mechanical cues on collagen matrix synthesis, the results indicated that VSMC biosynthetic behavior is indeed a function of global strain where the highest quantity of collagen production was observed at 30% strain. When specimens were subjected to the largest strain level of 50%, an lower net biosynthetic response was observed (Figures 4 and 5), with the 50% strain group producing a smaller collagen mass at day 7 and 14 when compared to the 30% group and a not-significantly different collagen mass at day 7 when compared to the day 0, static and 15% strain group. The 30% cyclic strain level cannot be claimed as the best optimal training for the most ECM synthesis, as a multitude of different inherent characteristics of each tissue engineering system play a role on dense connective tissue formation (e.g. type of deformation, frequency, cellular environment, scaffold-cell interactions, etc.). However, we observed that within our system, the 30% cyclic strain did stimulate better outcomes when compared with groups trained with other strain levels (15% and 50% strain) and with the static group. Thus, and with the objective of better understanding the outcome of finite deformation mechanical stimulation, the 30% strain group was further investigated at day 21.

The specific mechanism for this behavior, i.e. the most enhancement occurring with the 30% strain group while a subsequent suppression occurs at larger strain levels, is not known. We can speculate that large tractions or large cyclic strain amplitude (e.g. 50% cyclic strain) may be deleterious for constituent cells, resulting in a lag period of matrix production where cells are reorienting or altering their interaction with surrounding PEUU fibers to a more favorable stress state. Another plausible explanation could involve up regulation and production of matrix metalloproteinases (MMP) resulting in a competing effect, limiting new matrix deposition. Cyclic strain has been observed to induce MMP up regulation and release and is typically associated with active remodeling responses (Hasaneen et al. 2005; Haseneen et al. 2003; von Offenberg Sweeney et al. 2004). Cyclic strain appeared to induce sGAG production. However, this was not observed to be dependent on strain magnitude.

Recent literature shows that there is a wide array of scaffold materials and cell sources being actively investigated in efforts to produce functional engineered tissues (Mol et al. 2006; Nerurkar et al. 2011c; Sodian et al. 2000b). Related efforts with rapidly degrading scaffolds, such as non-woven PGA or fibrin gels, have shown the ability to produce anisotropic materials when combined with dynamic mechanical training (Kortsmit et al. 2009; Robinson et al. 2008). While encouraging, these approaches generally lack sufficient mechanical integrity the amount of de novo matrix proteins that can reasonably be attained within electrospun constructs at relatively short time periods represents a fairly small fraction of the total construct. In related studies by Nerurkar et al., the percent dry weight of collagen at 3–10 weeks for mesenchymal stem cells seeded in an electrospun PCL scaffolds was approximately 2–8% (Nerurkar et al. 2011a; Nerurkar et al. 2011b).

Biologically active constructs with sufficient mechanical function are critical to facilitate host acceptance and integration (Badylak 2007), and to withstand the biomechanical environment of heart valve leaflet tissues (Sacks et al. 2009a), not only acutely but also long-term. The present results indicate, for the first time, that finite deformation training is capable of promoting the production of a robust matrix phase that exhibits material properties approaching that of clinically relevant tissues for heart valve replacement. However, fully recapitulating all biological and mechanical characteristics of healthy native tissues is well beyond our current understanding.

4.2 - Collagen synthesis and the role of mechanical deformations

In our preliminary studies (Supplemental Figure 1) collagen fibers were identified as the most relevant structural ECM component for this study. Single collagen fibers are generally characterized by elastic moduli orders of magnitude larger than elastin fibers. For example, while Wenger et al. (Wenger et al. 2007) reported elastic moduli range of 5 GPa −11.5 GPa for individual rat tail tendon type 1 collagen, Aron et. al. (Aaron and Gosline 1981) measured an elastic modulus of 0.41 MPa for single elastin fibers derived from bovine ligamentum nuchae of mature beef cattle. Therefore, the same given level of mechanical strain would result in a limited contribution of elastin to the transmitted force. Previous studies by Englemayr et al. (Engelmayr et al. 2005; Engelmayr and Sacks 2008; Engelmayr et al. 2006) with VSMCs seeded on needled-non-woven scaffold undergoing cyclic flexure (which translate to small strain stimuli and does not impart the substantial enhancement in ECM production we report with this finite deformation training) similarly demonstrated that elastin was not observed histologically or biochemically after 30h or 3 weeks. Movat pentachrome stained sections revealed the ECM to consist of proteoglycans with sparse aggregates of collagen (63% increase compared with the static control group), and immunohistochemical staining revealed increases in vimentin expression (with respect to the static control group) and comparable SMC α-actin. Vimentin is well known for maintaining cell shape and stabilizing cytoskeletal interactions, and its expression may corroborate the direct effect of dynamic mechanical stimulation on VSMC proliferation, phenotype, and synthetic behavior.

In addition, the necessity of undergoing large deformations affects the capacity of an engineered construct to recapitulate native mechanics (Sodian et al. 2000a), preserve

underlying tissue geometry and functional parameters with a cardiac patch (Fujimoto et al. 2007) or match bordering tissue compliance (Nieponice et al. 2008; Takanari et al. 2013). While flow and pressure have been adopted to augment tissue formation to some extent, animal studies have proved that this class of conditioning stimuli still does not provide sufficient mechanical strength for mechanically demanding scenarios such as TEHVs in the aortic position. This limitation was significantly mitigated by shifting from small (2%) to large (15%) strain conditioning modalities (Mol et al. 2003), and these results are in agreement with our study which confirms the existence of a strain dependence mechanism and identifies 30% strain level as suitable to enhance ECM formation. Furthermore, large deformations are generally combined with chemical stimuli and this interplay might induce a synergistic increase of collagen mass (Huey and Athanasiou 2011).

However, the scaffolds and bioreactors typically adopted (de Jonge et al. 2013b; Huey and Athanasiou 2011; Kim et al. 1999) are limited by strain ranges of about 20% and large strains have not been fully investigated due to the lack of appropriate bioreactor and scaffold technologies. Materials chosen for tissue engineered pulmonary valve scaffolds (Sacks et al. 2009b) have often been non-woven fabrics that are remarkably stiff compared to the native tissue (Hoerstrup et al. 2000). Similarly, gel-based engineered constructs are relevant to investigate tissue remodeling under in vitro conditioning regimens; however, their uniaxial or biaxial mechanical response remain substantially more compliant than the native tissue (de Jonge et al. 2013a).

The non-affine (Chandran and Barocas 2006; Sander and Barocas 2009) {Carleton, 2015 #63} and heterogeneous nature (Stella et al. 2010) of the strain transfer mechanism makes the adoption of continuum theory intractable and indicates the implementation of either structural statistic (Courtney et al. 2006) or structural determinist (Argento et al. 2012; Stylianopoulos and Barocas 2007b) approaches. While nuclear aspect ratio (Guilak et al. 1995; Thomas et al. 2002), cellular aspect ratio (Lee et al. 2015) or single fiber stretch (Lanir 2014) have been successfully utilized, a definitive metric for cell-scaffold mechanotransduction has not been identified. In addition, organ level strain does not translate directly to equivalent deformation at the cellular level as the strain transfer process is highly dependent on tissue micro-architecture topology (Stella et al. 2008). Finally, the dynamic characteristics of the conditioning regimen loading pattern, specifically the frequency of cyclic stimuli, adds another layer of complexity with static (negligible to mild effects) and dynamic deformations around 1 Hz (major effects) being significantly different (Mol et al. 2006; Rubbens et al. 2009) in terms affecting cross-link densities, mechanics, collagen production and organization.

While numerical models have remarkably increased their predictive capacity at different scale lengths (Argento et al. 2012; Martinac 2014; Sander et al. 2009; Stylianopoulos and Barocas 2007c; Stylianopoulos and Barocas 2007d) only few attempts have successfully modeled scaffold fiber networks and non-fibrillar matrix interactions (Aghvami et al. 2013; Breuls et al. 2002). More importantly, none of these studies showed the ability to de-couple scaffold fiber networks from fibrillar ECM mechanics. In principle, de novo collagen mass can be quantified by biological assay (Brown et al. 2000), similarly collagen network structure can be studied by imaging techniques such as confocal (Stella et al. 2008) or multi-

photon microscopy (D'Amore et al. 2014). However, these types of data do not provide any information on the mechanical properties. Ultimately, the evolving mechanical characteristics of the de novo ECM must be quantifiable, predictable, and designed for.

4.3 - Evaluation of the de novo collagen mechanical properties

Biaxial tests (Figure 7a and 7b) of engineered tissue constructs before and after trypsin degradation allowed elimination of the contribution of the ECM component without affecting PEUU scaffold mechanics. The validity of assumptions in Equation (2) has been verified with the technique previously employed by Engelmayr et al. (Engelmayr and Sacks 2008) for polyacrylamide (PAM) gel infiltrated in needled-non-woven 50:50 PGA/PLLA scaffolds. PAM gels of known elastic modulus were utilized to simulate ECM elaboration inside the PEUU electrospun scaffold at different levels of gel infiltration (specifically with 20.7% PAM). Removal of the PAM gel component from the gel-infiltrated scaffold resulted in an isotropic reduction in the elastic stored energy density of the form $\psi_{PAM} = C_1(I_1 - 3)+C_2(I_2 - 3)$ with $\mu_{PAM} = (C_1 + C_2) / 2$ equal to the known PAM gel elastic modulus (predicted 53.83 ± 2.45 kPa to 51.1 kPa known). This suggested both lack of gel-scaffold mechanical interaction and the additive properties of the stored energy density of each component.

Estimation of biaxial material properties from matrix strain energy data (Figure 8a and 8b) suggested that the formed matrix elements created a mildly anisotropic phase (Figures 8a and 8c). The ECM component was stiffer along the XD (Figure 8c, red lines) whereas the PEUU component alone showed isotropic characteristic after 3 weeks of conditioning (Figure 8c, blue lines). Overall, this suggested that the main direction of the strain (XD) induced higher alignment of not only the scaffold fibers, but also of the de novo collagen fibers along the direction of the mechanical conditioning.

This phenomenon has recently been reported in other electrospun fibrous constructs aimed at recapitulating intervertebral disk characteristics (Nerurkar et al. 2011c). In that study, polycaprolactone (PCL) electrospun scaffolds were seeded with mesenchymal stem cells and maintained in static culture up to 10 weeks. Our group has also previously observed de novo ECM-fiber alignment on cell seeded non-woven PGA-PLLA scaffold blends (Engelmayr and Sacks 2008; Engelmayr et al. 2006) where the gross fiber orientation induced a micro-patterning effect on matrix elaboration within the construct. Results from the present study support that the newly formed matrix phase exhibited anisotropic stress-strain behaviors and elastic modulus (Table 2) qualitatively comparable to the response of glutaraldehyde fixed BP tissue (Figure 9). Glutaraldehyde fixed pericardial tissues is a clinically relevant material used for cardiovascular reconstruction and valve bioprostheses (Barbenel et al. 1987; Billiar and Sacks 2000a; Billiar and Sacks 2000b; Crofts and Trowbridge 1988; Langdon et al. 1999; Liao et al. 1992; Sacks and Chuong 1998), its mechanical response of has been well documented (Sacks and Chuong 1998), and serves the purpose of qualitative comparison with the de novo ECM mechanical response.

The structural constitutive modeling approach can describe and predict the mechanical response characterized by an anisotropic stored energy density function, and most importantly, allows for better interpretation and insight of the underlying characteristics of

tissues and their mechanistic effects. Application of the structural model to experimental data obtained with BP resulted in collagen fiber stiffness of ≈20 MPa per unit collagen volume fraction, highly aligned in the PD direction with 38 degree of fiber splay, 20% ± 3% ensemble strain recruitment range (cf. Table 2 and Fan and Sacks (Fan and Sacks 2014)), and properties comparable to a wide range of collagenous tissues. The mechanical properties of the de novo ECM can be compared with the properties of BP at two levels: (i) at the bulk level, its ability to store mechanical energy is comparable to BP particularly at lower strains (Figure 9), however it fails to show the common functionality of undulated collagenous tissues beyond the fiber recruitment range, i.e. steep increases of stress beyond certain strain levels; and (ii) microstructurally, although collagen fiber orientation of the engineered tissue is seemingly similar to native-like BP (with 34 degrees fiber splay), collagen fibers are apparently only half as stiff as the ones present in the untreated BP (Table 2). However, collagen fiber undulation of the de novo tissue seems to be minimal or non-existent, as can be observed by the mildly linear mechanical response of the de novo ECM and recruitment ranges obtained with the structural model fit – apparently collagen fibers are recruited at 0% strain (Table 2). Collagen fiber crimping and maturation is achieved with extensive recursive remodeling of the ECM in collagenous tissues, a phenomenon known to take place in much longer time scales than the 3 weeks considered in the current tissue engineering study (Vogel 1980). Notwithstanding, while engineered tissue efforts are still far away from the gold standard of fixed BP for construction of bioprosthetic heart valves, it was still possible to achieve not only a substantially increased production of ECM, but also an appealing augmentation of the quality of the ECM produced through strain modulation. Most importantly, this study represents an important step towards the ultimate goal of a achieving a fully functional and mechanically robust load bearing tissues – the ECM produced under large strain conditioning is considerable stiffer than previously obtained with small deformations by Englemayr et al. (Engelmayr and Sacks 2008) (Figure 9).

4.4 – Limitations

Imaging scaffold volume in an effort to quantify both 3D structure and embedded cell deformation adds complexity to the study of scaffold – cell interaction. The relative opacity of the vast majority of fibrous biomaterials did not allow for successful imaging (e.g. by confocal or multi-photon microscopy) at penetration depths > 50 μm (Stella et al. 2008). Moreover, while there is strong mechanical evidence that the newly formed collagen phase is anisotropic, we were unable to verify the structure visually. This is largely a result of practical limitations of preparing specimens for histological evaluation and limitations in imaging technology. While GMA and paraffin embedded specimens enabled reliable transverse sections, en face sectioning was found to be unsuccessful. Extensive cutting artifacts making imaging impossible confounded all efforts. In a similar light, it was assumed that matrix area fractions from transverse sections through the specimen are representative of overall volume fraction. Furthermore, confocal based imaging techniques were also unsuccessful. Two main characteristics prohibited detailed imaging of the matrix phase in situ. First, extensive cell proliferation at the specimen surface limited our ability to image deep enough into the specimen to investigate cell morphologies and matrix structure embedded within the scaffold structure. Also, the strong autofluorescent nature of PEUU resulted in substantial scattering of the signal, effectively masking matrix specific signals.

After dynamic culture, the constructs were observed to be less distensible without inducing damage. As a result, 3 discrete levels of deformation were investigated (15%, 30%, and 50%) reflecting the strain magnitudes imposed during in vitro dynamic culture. While it was possible to quantify the effects of large deformation on ECM elaboration and to model and predict de novo ECM mechanical response, the complex biomechanical interactions between micro-integrated VSMC and electrospun polymer scaffolds with corresponding biochemical effects remain largely unknown.

5 – CONCLUSIONS

To our knowledge, this is the first report to consider the effects of physiologically relevant large deformations (>30% strain) and the corresponding outcomes in terms of ECM mechanics. The current work affirmed the assertion that finite deformation plays a critical role in ECM production as well as in the stiffness of its constituents. Furthermore, the current investigation shows that it is possible to regulate biosynthetic activity and assess the production of a collagenous matrix exhibiting robust mechanical properties and anisotropy via exogenous mechanical cues even at relatively short experimental time points. We conclude that large deformations can play a critical role not only in the quantity of ECM synthesis (i.e. the rate of mass production), but also on the quality of the newly formed ECM constituents (i.e. their stiffness). The improved understanding of the process of growth and development of ECM in these mechano-sensitive cell-scaffold systems will lead to more rational design and manufacturing of engineered tissues operating under highly demanding mechanical environments.

Supplementary Material

Refer to Web version on PubMed Central for supplementary material.

Acknowledgments

This work was financially supported by the National Institutes of Health (NHLBI Grant R01 HL-068816 and R01 HL-089750), the RiMED Foundation (RiMED fellow research support grant to Antonio D'Amore).

BIBLIOGRAPHY

Aaron BB, Gosline JM. Elastin as a random-network elastomer: A mechanical and optical analysis of single elastin fibers. Biopolymers. 1981; 20:1247–1260.

Aggarwal, A.; Aguilar, VS.; Lee, C-H.; Ferrari, G.; Gorman, JH.; Gorman, RC.; Sacks, MS. Patient-Specific Modeling of Heart Valves: From Image to Simulation. In: Ourselin, S.; Rueckert, D.; Smith, N., editors. Proceedings; Functional Imaging and Modeling of the Heart: 7th International Conference, FIMH 2013; June 20–22, 2013; London, UK. Berlin, Heidelberg: Springer Berlin Heidelberg; 2013. p. 141-149.

Aggarwal, A.; Sacks, MS. A Framework for Determination of Heart Valves' Mechanical Properties Using Inverse-Modeling Approach. In: van Assen, H.; Bovendeerd, P.; Delhaas, T., editors. Proceedings; Functional Imaging and Modeling of the Heart: 8th International Conference, FIMH 2015; June 25–27, 2015; Maastricht, The Netherlands. Springer; 2015a. p. 285-294.

Aggarwal A, Sacks MS. An inverse modeling approach for semilunar heart valve leaflet mechanics: exploitation of tissue structure. Biomechanics and modeling in mechanobiology. 2015b:1–24. [PubMed: 24718853]

Aghvami M, Barocas VH, Sander EA. Multiscale mechanical simulations of cell compacted collagen gels. J Biomech Eng. 2013; 135:71004. [PubMed: 23720151]

Amoroso NJ, D'Amore A, Hong Y, Rivera CP, Sacks MS, Wagner WR. Microstructural manipulation of electrospun scaffolds for specific bending stiffness for heart valve tissue engineering. Acta biomaterialia. 2012; 8:4268–4277. [PubMed: 22890285]

Amoroso NJ, D'Amore A, Hong Y, Wagner WR, Sacks MS. Elastomeric electrospun polyurethane scaffolds: the interrelationship between fabrication conditions, fiber topology, and mechanical properties. Adv Mater. 2011; 23:106–111. [PubMed: 20979240]

Argento G, Simonet M, Oomens CW, Baaijens FP. Multi-scale mechanical characterization of scaffolds for heart valve tissue engineering. J Biomech. 2012; 45:2893–2898. [PubMed: 22999107]

Badylak S. The extracellular matrix as a biologic scaffold material. Biomaterials. 2007; 28:3587–3593. [PubMed: 17524477]

Baker BM, Gee AO, Metter RB, Nathan AS, Marklein RA, Burdick JA, Mauck RL. The potential to improve cell infiltration in composite fiber-aligned electrospun scaffolds by the selective removal of sacrificial fibers. Biomaterials. 2008; 29:2348–2358. [PubMed: 18313138]

Barbenel, JC.; Zioupos, P.; Fisher, J. The mechanical properties of bovine pericardium. In: Pizzoferrato, A.; Marchetti, PG.; Ravagliolin, A.; Lee, AJC., editors. Biomaterials and Clinical Application. Amsterdam: Elsevier; 1987. p. 421

Bassett CA, Pawluk RJ, Pilla AA. Acceleration of fracture repair by electromagnetic fields. A surgically noninvasive method. Ann N Y Acad Sci. 1974; 238:242–262. [PubMed: 4548330]

Billiar KL, Sacks MS. Biaxial mechanical properties of the native and glutaraldehyde-treated aortic valve cusp: Part II--A structural constitutive model. J Biomech Eng. 2000a; 122:327–335. [PubMed: 11036555]

Billiar KL, Sacks MS. Biaxial mechanical properties of the natural and glutaraldehyde treated aortic valve cusp - Part I: Experimental results. J Biomech Eng-T Asme. 2000b; 122:23–30. doi:

Breuls RG, Sengers BG, Oomens CW, Bouten CV, Baaijens FP. Predicting local cell deformations in engineered tissue constructs: a multilevel finite element approach. J Biomech Eng. 2002; 124:198–207. [PubMed: 12002129]

Brown AN, Kim BS, Alsberg E, Mooney DJ. Combining chondrocytes and smooth muscle cells to engineer hybrid soft tissue constructs. Tissue Eng. 2000; 6:297–305. [PubMed: 10992427]

Chandran PL, Barocas VH. Affine versus non-affine fibril kinematics in collagen networks: theoretical studies of network behavior. J Biomech Eng. 2006; 128:259–270. [PubMed: 16524339]

Courtney T, Sacks MS, Stankus J, Guan J, Wagner WR. Design and analysis of tissue engineering scaffolds that mimic soft tissue mechanical anisotropy. Biomaterials. 2006; 27:3631–3638. [PubMed: 16545867]

Crofts CE, Trowbridge EA. The tensile strength of natural and chemically modified bovine pericardium. Journal of Biomedical Materials Research. 1988; 22:89–98. [PubMed: 3128550]

D'Amore A, et al. From single fiber to macro-level mechanics: A structural finite-element model for elastomeric fibrous biomaterials. J Mech Behav Biomed Mater. 2014; 39:146–161. [PubMed: 25128869]

D’Amore A, et al. From single fiber to macro-level mechanics: A structural finite-element model for elastomeric fibrous biomaterials. J Mech Behav Biomed Mater. 2014; 39:146–161. [PubMed: 25128869]

de Jonge N, Kanters FM, Baaijens FP, Bouten CV. Strain-induced collagen organization at the micro-level in fibrin-based engineered tissue constructs. Ann Biomed Eng. 2013a; 41:763–774. [PubMed: 23184346]

de Jonge N, Muylaert DE, Fioretta ES, Baaijens FP, Fledderus JO, Verhaar MC, Bouten CV. Matrix production and organization by endothelial colony forming cells in mechanically strained engineered tissue constructs. PLoS ONE. 2013b; 8:e73161. [PubMed: 24023827]

Duarte LR. The stimulation of bone growth by ultrasound. Arch Orthop Trauma Surg. 1983; 101:153–159. [PubMed: 6870502]

Engelmayr GC Jr, Rabkin E, Sutherland FW, Schoen FJ, Mayer JE Jr, Sacks MS. The independent role of cyclic flexure in the early in vitro development of an engineered heart valve tissue. Biomaterials. 2005; 26:175–187. [PubMed: 15207464]

Engelmayr GC Jr, Sacks MS. Prediction of extracellular matrix stiffness in engineered heart valve tissues based on nonwoven scaffolds. Biomech Model Mechanobiol. 2008; 7:309–321. [PubMed: 17713801]

Engelmayr GC Jr, Sales VL, Mayer JE Jr, Sacks MS. Cyclic flexure and laminar flow synergistically accelerate mesenchymal stem cell-mediated engineered tissue formation: Implications for engineered heart valve tissues. Biomaterials. 2006; 27:6083–6095. [PubMed: 16930686]

Fan R, Bayoumi AS, Chen P, Hobson CM, Wagner WR, Mayer JE Jr, Sacks MS. Optimal elastomeric scaffold leaflet shape for pulmonary heart valve leaflet replacement. J Biomech. 2013a; 46:662–669. [PubMed: 23294966]

Fan R, Bayoumi AS, Chen P, Hobson CM, Wagner WR, Mayer JE Jr, Sacks MS. Optimal elastomeric scaffold leaflet shape for pulmonary heart valve leaflet replacement. Journal of Biomechanics. 2013b; 46:662–669. doi:http://dx.doi.org/10.1016/j.jbiomech.2012.11.046. [PubMed: 23294966]

Fan R, Sacks MS. Simulation of planar soft tissues using a structural constitutive model: finite element implementation and validation. J Biomech. 2014; 47:2043–2054. [PubMed: 24746842]

Fata B, Zhang W, Amini R, Sacks M. Insights into Regional Adaptations in the Growing Pulmonary Artery Using a Meso-Scale Structural Model: Effects of Ascending Aorta Impingement. J Biomech Eng. 2014

Fujimoto KL, et al. An elastic, biodegradable cardiac patch induces contractile smooth muscle and improves cardiac remodeling and function in subacute myocardial infarction. J Am Coll Cardiol. 2007; 49:2292–2300. [PubMed: 17560295]

Guan J, Sacks MS, Beckman EJ, Wagner WR. Biodegradable poly(ether ester urethane)urea elastomers based on poly(ether ester) triblock copolymers and putrescine: synthesis, characterization and cytocompatibility. Biomaterials. 2004; 25:85–96. [PubMed: 14580912]

Guilak F, Ratcliffe A, Mow VC. Chondrocyte deformation and local tissue strain in articular cartilage: a confocal microscopy study. PG - 410-21. J Orthop Res. 1995; 13

Hahn MS, McHale MK, Wang E, Schmedlen RH, West JL. Physiologic pulsatile flow bioreactor conditioning of poly(ethylene glycol)-based tissue engineered vascular grafts. Ann Biomed Eng. 2007; 35:190–200. [PubMed: 17180465]

Hasaneen NA, Zucker S, Cao J, Chiarelli C, Panettieri RA, Foda HD. Cyclic mechanical strain-induced proliferation and migration of human airway smooth muscle cells: role of EMMPRIN and MMPs. FASEB J. 2005; 19:1507–1509. [PubMed: 16014803]

Haseneen NA, Vaday GG, Zucker S, Foda HD. Mechanical stretch induces MMP-2 release and activation in lung endothelium: role of EMMPRIN. Am J Physiol Lung Cell Mol Physiol. 2003; 284:L541–L547. [PubMed: 12456388]

Hoerstrup SP, et al. Functional living trileaflet heart valves grown In vitro. Circulation. 2000; 102:III44–III49. [PubMed: 11082361]

Huey DJ, Athanasiou KA. Tension-compression loading with chemical stimulation results in additive increases to functional properties of anatomic meniscal constructs. PLoS ONE. 2011; 6:e27857. [PubMed: 22114714]

Kim BS, Nikolovski J, Bonadio J, Mooney DJ. Cyclic mechanical strain regulates the development of engineered smooth muscle tissue. Nat Biotechnol. 1999; 17:979–983. [PubMed: 10504698]

Kim YJ, Sah RL, Doong JY, Grodzinsky AJ. Fluorometric assay of DNA in cartilage explants using Hoechst 33258. Anal Biochem. 1988; 174:168–176. [PubMed: 2464289]

Kortsmit J, Rutten MC, Wijlaars MW, Baaijens FP. Deformation-controlled load application in heart valve tissue engineering. Tissue engineering Part C, Methods. 2009; 15:707–716. [PubMed: 19275473]

Langdon SE, Chernecky R, Pereira CA, Abdulla D, Lee JM. Biaxial mechanical/structural effects of equibiaxial strain during crosslinking of bovine pericardial xenograft materials. Biomaterials. 1999; 20:137–153. [PubMed: 10022783]

Lanir Y. Mechanistic micro-structural theory of soft tissues growth and remodeling: tissues with unidirectional fibers. Biomechanics and modeling in mechanobiology. 2014:1–22.

Lee CH, Carruthers CA, Ayoub S, Gorman RC, Gorman JH 3rd, Sacks MS. Quantification and simulation of layer-specific mitral valve interstitial cells deformation under physiological loading. J Theor Biol. 2015

Lee CH, Shin HJ, Cho IH, Kang YM, Kim IA, Park KD, Shin JW. Nanofiber alignment and direction of mechanical strain affect the ECM production of human ACL fibroblast. Biomaterials. 2005; 26:1261–1270. [PubMed: 15475056]

Liao K, Seifter E, Hoffman D, Yellin EL, Frater RW. Bovine pericardium versus porcine aortic valve: comparison of tissue biological properties as prosthetic valves. Artif Organs. 1992; 16:361–365. [PubMed: 10078275]

Martinac B. The ion channels to cytoskeleton connection as potential mechanism of mechanosensitivity. Biochim Biophys Acta. 2014; 1838:682–691. [PubMed: 23886913]

Merryman WD, Lukoff HD, Long RA, Engelmayr GC Jr, Hopkins RA, Sacks MS. Synergistic effects of cyclic tension and transforming growth factor-beta1 on the aortic valve myofibroblast. Cardiovasc Pathol. 2007; 16:268–276. doi:S1054-8807(07)00053-1 [pii] 10.1016/j.carpath.2007.03.006. [PubMed: 17868877]

Mol A, et al. The relevance of large strains in functional tissue engineering of heart valves. Thorac Cardiovasc Surg. 2003; 51:78–83. [PubMed: 12730815]

Mol A, Driessen NJ, Rutten MC, Hoerstrup SP, Bouten CV, Baaijens FP. Tissue engineering of human heart valve leaflets: a novel bioreactor for a strain-based conditioning approach. Ann Biomed Eng. 2005; 33:1778–1788. [PubMed: 16389526]

Mol A, Rutten MC, Driessen NJ, Bouten CV, Zund G, Baaijens FP, Hoerstrup SP. Autologous human tissue-engineered heart valves: prospects for systemic application. Circulation. 2006; 114:I152–I158. [PubMed: 16820565]

Nerurkar NL, Han W, Mauck RL, Elliott DM. Homologous structure-function relationships between native fibrocartilage and tissue engineered from MSC-seeded nanofibrous scaffolds. Biomaterials. 2011a; 32:461–468. [PubMed: 20880577]

Nerurkar NL, Mauck RL, Elliott DM. Modeling interlamellar interactions in angle-ply biologic laminates for annulus fibrosus tissue engineering. Biomech Model Mechanobiol. 2011b; 10:973–984. [PubMed: 21287395]

Nerurkar NL, Sen S, Baker BM, Elliott DM, Mauck RL. Dynamic culture enhances stem cell infiltration and modulates extracellular matrix production on aligned electrospun nanofibrous scaffolds. Acta biomaterialia. 2011c; 7:485–491. [PubMed: 20728589]

Nieponice A, Soletti L, Guan J, Deasy BM, Huard J, Wagner WR, Vorp DA. Development of a tissue-engineered vascular graft combining a biodegradable scaffold, muscle-derived stem cells and a rotational vacuum seeding technique. Biomaterials. 2008; 29:825–833. [PubMed: 18035412]

Robinson PS, Johnson SL, Evans MC, Barocas VH, Tranquillo RT. Functional tissue-engineered valves from cell-remodeled fibrin with commissural alignment of cell-produced collagen. Tissue Eng Part A. 2008; 14:83–95. [PubMed: 18333807]

Rubbens MP, Mol A, Boerboom RA, Bank RA, Baaijens FP, Bouten CV. Intermittent straining accelerates the development of tissue properties in engineered heart valve tissue. Tissue Eng Part A. 2009; 15:999–1008. [PubMed: 18795866]

Sacks MS, Chuong CJ. Orthotropic mechanical properties of chemically treated bovine pericardium. Ann Biomed Eng. 1998; 26:892–902. [PubMed: 9779962]

Sacks MS, Merryman WD, Schmidt DE. On the biomechanics of heart valve function. J Biomech. 2009a; 42:1804–1824. doi:S0021-9290(09)00265-6 [pii] 10.1016/j.jbiomech.2009.05.015. [PubMed: 19540499]

Sacks MS, Schoen FJ, Mayer JE. Bioengineering challenges for heart valve tissue engineering. Annu Rev Biomed Eng. 2009b; 11:289–313. [PubMed: 19413511]

Sander EA, Barocas VH. Comparison of 2D fiber network orientation measurement methods. Journal of Biomedical Materials Research Part A. 2009; 88A:322–331. [PubMed: 18286605]

Sander EA, Stylianopoulos T, Tranquillo RT, Barocas VH. Image-based multiscale modeling predicts tissue-level and network-level fiber reorganization in stretched cell-compacted collagen gels. Proc Natl Acad Sci U S A. 2009; 106:17675–17680. [PubMed: 19805118]

Seliktar D, Black RA, Vito RP, Nerem RM. Dynamic mechanical conditioning of collagen-gel blood vessel constructs induces remodeling in vitro. Ann Biomed Eng. 2000; 28:351–362. [PubMed: 10870892]

Soares JS, Sacks MS. A triphasic constrained mixture model of engineered tissue formation under in vitro dynamic mechanical conditioning. Biomech Model Mechanobiol. 2015

Sodian R, et al. Early In vivo experience with tissue-engineered trileaflet heart valves. Circulation. 2000a; 102:III22–III29. [PubMed: 11082357]

Sodian R, Sperling JS, Martin DP, Egozy A, Stock U, Mayer JE Jr, Vacanti JP. Fabrication of a trileaflet heart valve scaffold from a polyhydroxyalkanoate biopolyester for use in tissue engineering. Tissue Eng. 2000b; 6:183–188. [PubMed: 10941212]

Stankus JJ, Guan J, Fujimoto K, Wagner WR. Microintegrating smooth muscle cells into a biodegradable, elastomeric fiber matrix. Biomaterials. 2006; 27:735–744. [PubMed: 16095685]

Stankus JJ, Guan J, Wagner WR. Fabrication of biodegradable elastomeric scaffolds with sub-micron morphologies. J Biomed Mater Res. 2004; 70A:603–614.

Stella JA, Liao J, Hong Y, David Merryman W, Wagner WR, Sacks MS. Tissue-to-cellular level deformation coupling in cell micro-integrated elastomeric scaffolds. Biomaterials. 2008; 29:3228–3236. doi:S0142-9612(08)00260-3 [pii]10.1016/j.biomaterials.2008.04.029. [PubMed: 18472154]

Stella JA, Wagner WR, Sacks MS. Scale-dependent fiber kinematics of elastomeric electrospun scaffolds for soft tissue engineering. Journal of Biomedical Materials Research Part A. 2010; 93:1032–1042. [PubMed: 19753623]

Stylianopoulos T, Barocas V. Volume-Averaging Theory for the Study of the Mechanics of Collagen Networks. Comput Method Appl M. 2007a; 196:2981–2990.

Stylianopoulos T, Barocas VH. Multiscale, Structure-Based Modeling for the Elastic Mechanical Behavior of Arterial Walls. Journal of Biomechanical Engineering. 2007b; 129:611–618. [PubMed: 17655483]

Stylianopoulos T, Barocas VH. Multiscale, structure-based modeling for the elastic mechanical behavior of arterial walls. J Biomech Eng. 2007c; 129:611–618. [PubMed: 17655483]

Stylianopoulos T, Barocas VH. Volume-averaging theory for the study of the mechanics of collagen networks. Comput Meth Appl Mech Eng. 2007d; 196:2981–2990.

Syedain ZH, Tranquillo RT. Controlled cyclic stretch bioreactor for tissue-engineered heart valves. Biomaterials. 2009; 30:4078–4084. doi:S0142-9612(09)00403-7 [pii] 10.1016/j.biomaterials.2009.04.027. [PubMed: 19473698]

Syedain ZH, Weinberg JS, Tranquillo RT. Cyclic distension of fibrin-based tissue constructs: evidence of adaptation during growth of engineered connective tissue. Proc Natl Acad Sci U S A. 2008; 105:6537–6542. doi:0711217105 [pii] 10.1073/pnas.0711217105/. [PubMed: 18436647]

Takanari K, et al. Abdominal wall reconstruction by a regionally distinct biocomposite of extracellular matrix digest and a biodegradable elastomer. J Tissue Eng Regen Med. 2013

Thomas CH, Collier JH, Sfeir CS, Healy KE. Engineering gene expression and protein synthesis by modulation of nuclear shape. Proc Natl Acad Sci U S A. 2002; 99:1972–1977. [PubMed: 11842191]

Vogel HG. Influence of maturation and aging on mechanical and biochemical properties of connective tissue in rats. 1980; 14:283–292.

von Offenberg Sweeney N, Cummins PM, Birney YA, Cullen JP, Redmond EM, Cahill PA. Cyclic strain-mediated regulation of endothelial matrix metalloproteinase-2 expression and activity. Cardiovasc Res. 2004; 63:625–634. [PubMed: 15306218]

Wenger MPE, Bozec L, Horton MA, Mesquida P. Mechanical Properties of Collagen Fibrils. Biophysical Journal. 2007; 93:1255–1263. doi:http://dx.doi.org/10.1529/biophysj.106.103192. [PubMed: 17526569]

Zhang W, Ayoub S, Liao J, Sacks MS. On the mechanical role of collagen and elastin fibers in the layers of the mitral heart valve leaflet. J Mech Behav Biomed Mater. (in press).

Zhang W, Feng Y, Lee CH, Billiar KL, Sacks MS. A generalized method for the analysis of planar biaxial mechanical data using tethered testing configurations. J Biomech Eng. 2015; 137:064501. [PubMed: 25429606]

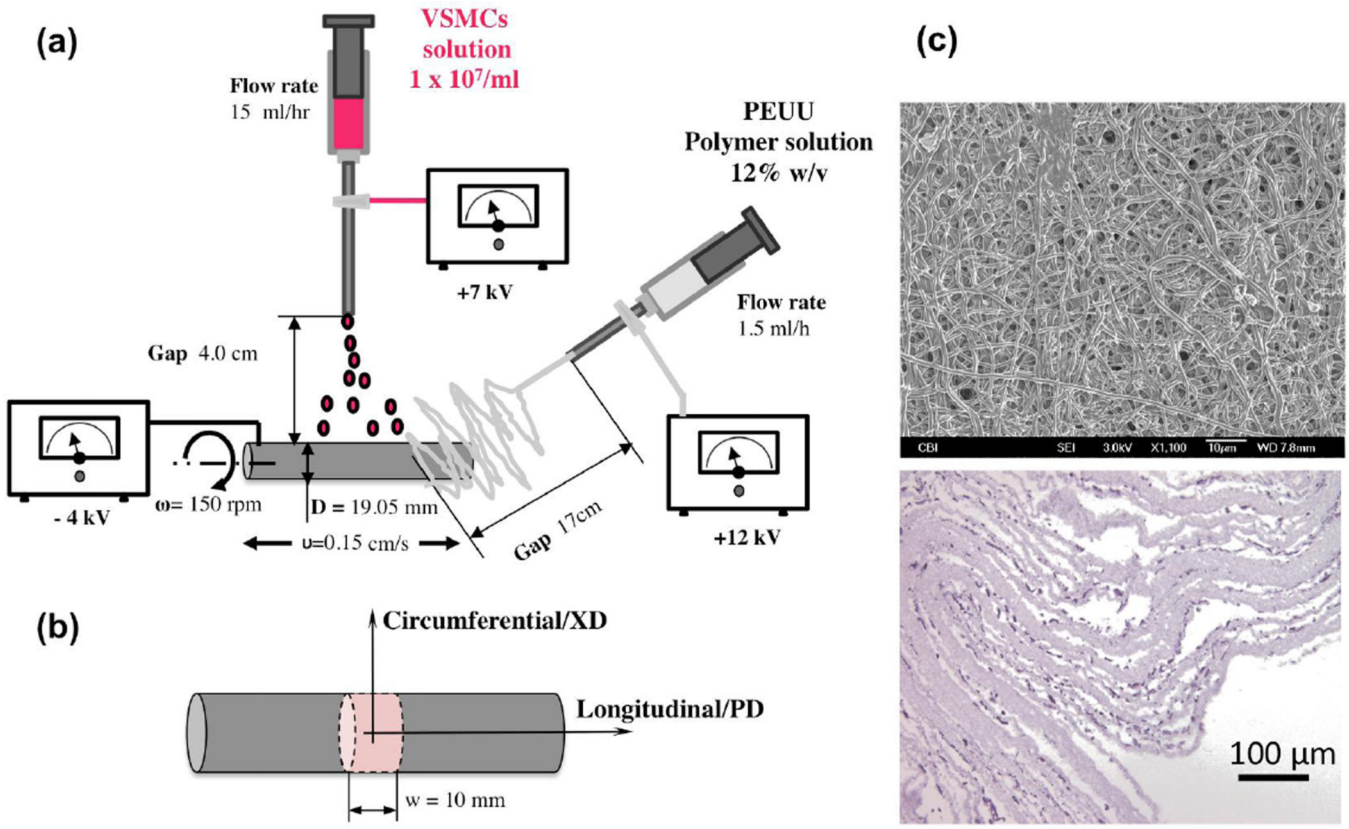

Figure 1.

A) Electrospinning device utilized in the study with related fabrication variables. B) sample reference systems adopted. C) SEM image of cell-seeded PEUU scaffold and representative cross section H&E staining.

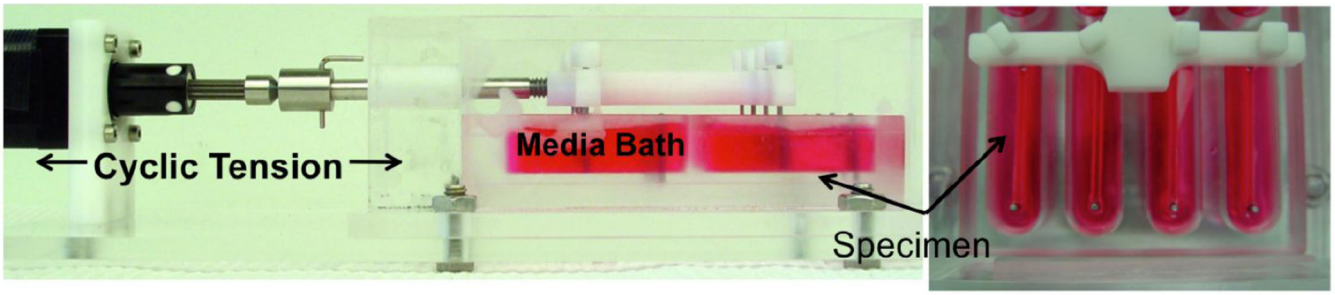

Test matrix

- 0, 7, 14, and 21 day endpoints
- 15%, 30%, and 50% strain groups (duty cycle of 1 Hz)

Biochemical assessment

- DNA (PicoGreen dsDNA, Molecular Probes)
- Collagen (Sircol™, Biocolor)
- Sulfated glycosaminoglycans (sGAG, Blyscan™, Biocolor)

Histological assessment

- Hematoxyn & Eosin (morphology)
- Picrosirius red (collagen)

Mechanical assessment

- Planar biaxial behavior (7 stress ratio controlled protocols)

Figure 2.

A) Stretch bioreactor loaded with specimen rings under uniaxial tension, conditioning regimen variables and sample testing summary

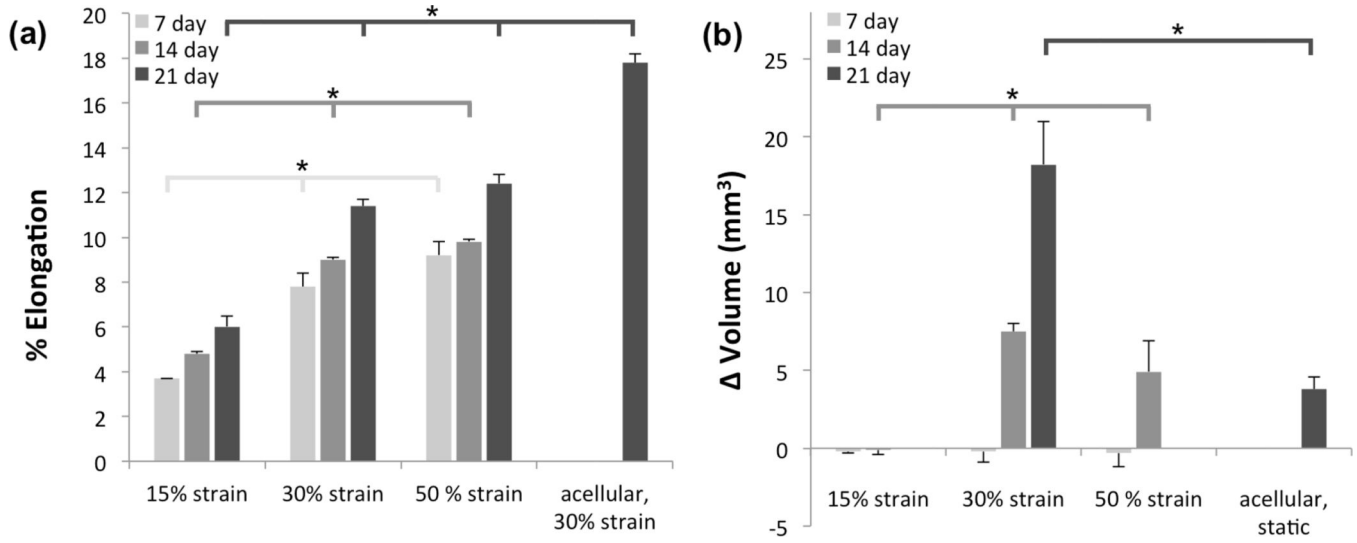

Figure 3.

A) Sample elongation and B) volume changes for different strain levels and time points. Differences in elongation resulting from each conditioning regime were statistically significant at all time points. Volumetric changes were not noticeable after 7 days, however statistical significance was observed for volumetric changes at 14 days with all conditioning protocols.

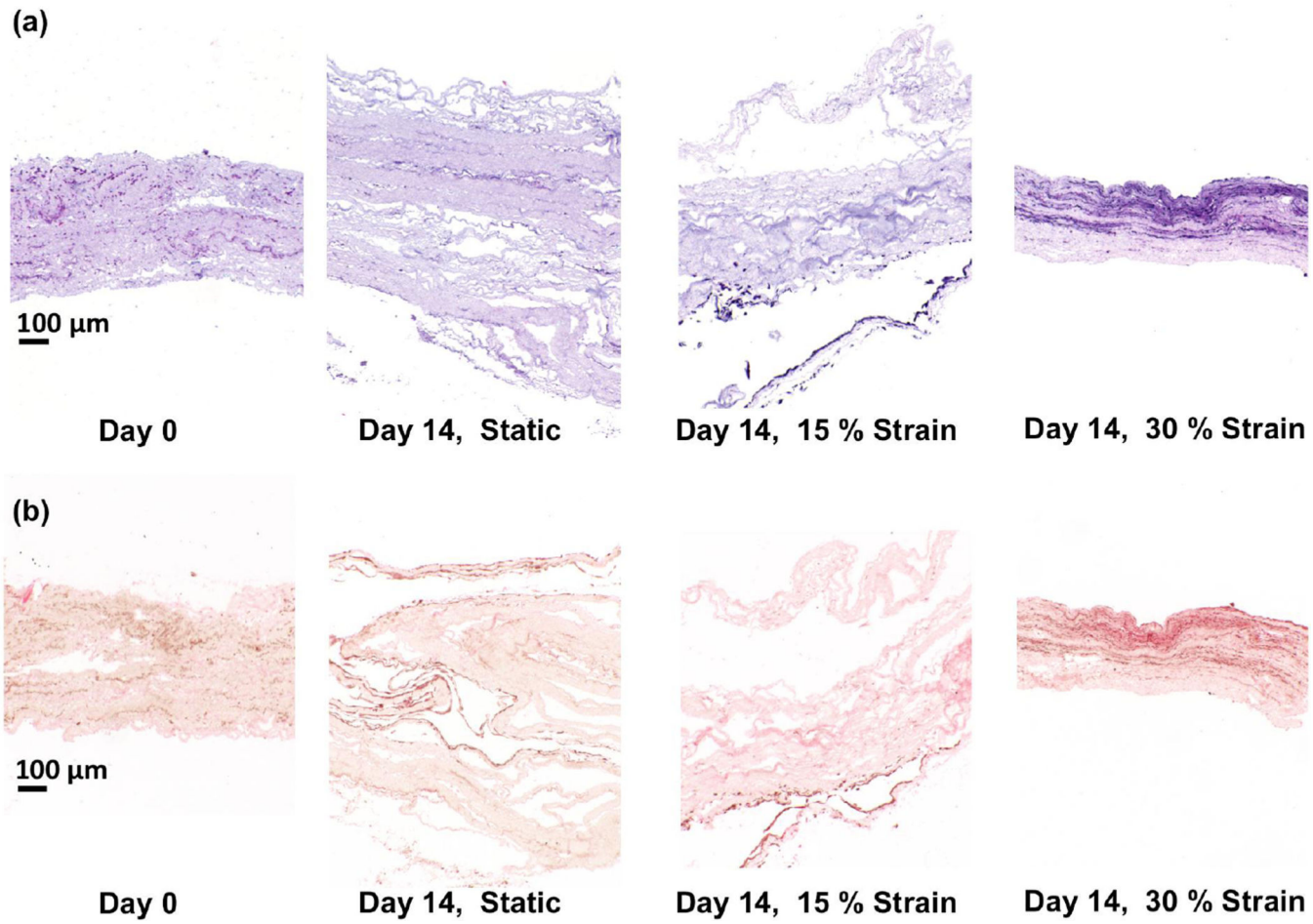

Figure 4.

A) H&E and B) picrosirius red staining of specimens conditioned for 14 days under static conditions and at 15% and 30% cyclic strain. Specimens at day 0 are included as the control group.

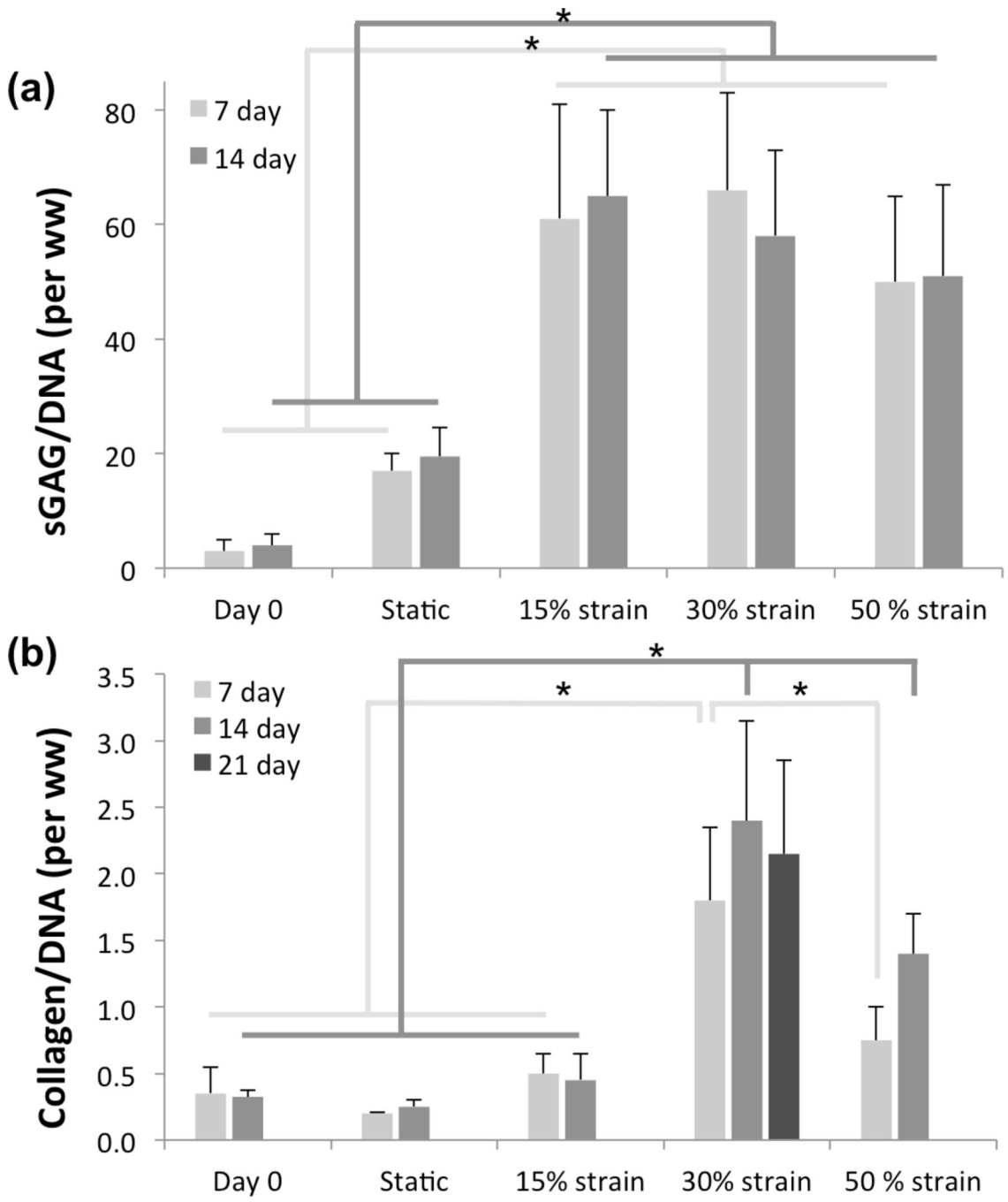

Figure 5.

A) Collagen and B) GAG synthesis as a function of finite deformation stimulation and time. Differences on sGAG deposition with cyclic strain conditioned are significantly different from the regime and at day 0. sGAG deposition dynamic condition is not significantly different among strain levels, as well as the static regime does not achieve significant difference from the day 0 control. Collagen deposition under static an 15% cyclic strain is not significantly different from the control group, however significant difference are observed in between 30% and 50% cyclic strain at day 7 and day 21.

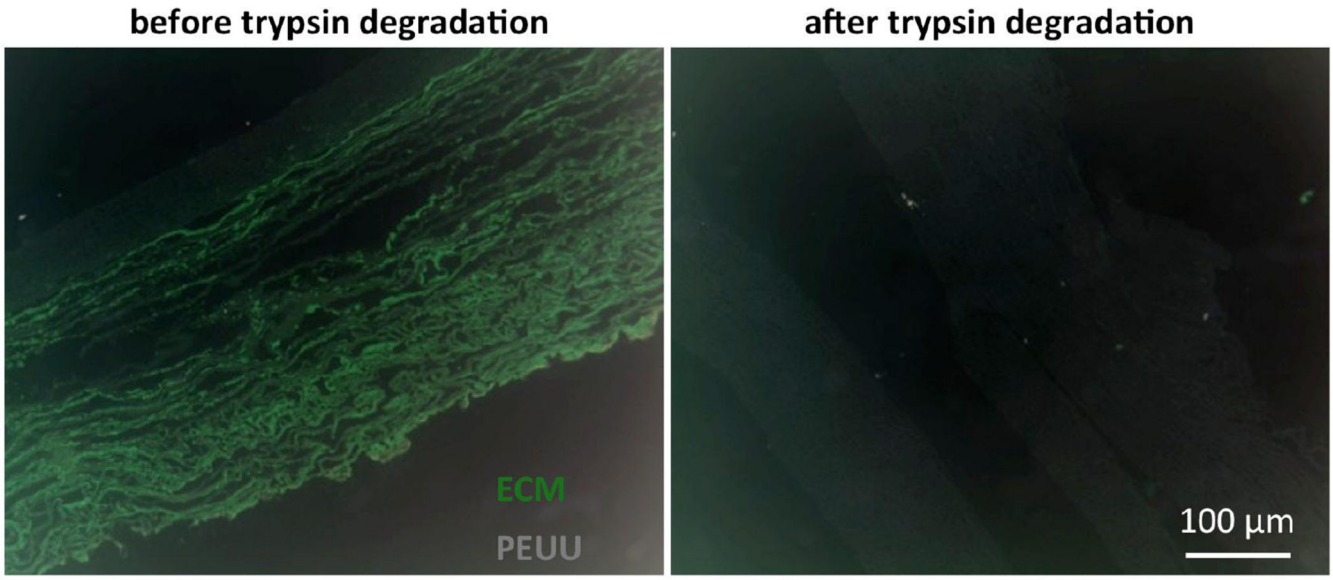

Figure 6.
Polymer and ECM components for 21 day samples before and after the ECM removal protocol by trypsin degradation.

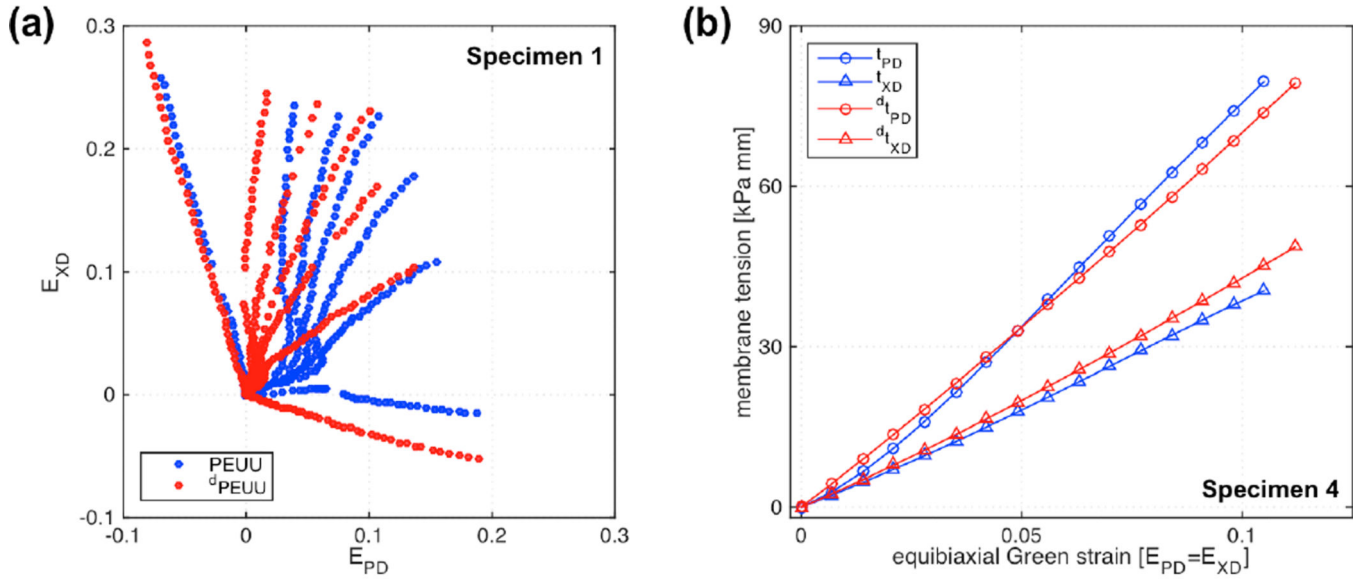

(c)

Specimen	1	2	3	4	5
$\int [t_{PD}(E) - {}^{d}t_{PD}(E)]^2 / [t_{PD}(E)]^2 \, dE$	0.0329	0.0356	0.0326	0.0049	0.0573
$\int [t_{XD}(E) - {}^{d}t_{XD}(E)]^2 / [t_{XD}(E)]^2 \, dE$	0.0336	0.0638	0.0757	0.0108	0.0024

Figure 7.

Mechanical effects of trypsin degradation on the PEUU component A) seven protocol tests before and after degradation on one representative sample, B) membrane tension response under equi-strain conditions for a representative sample, C) membrane tension vs. Green' strain areas differences for all of the samples.

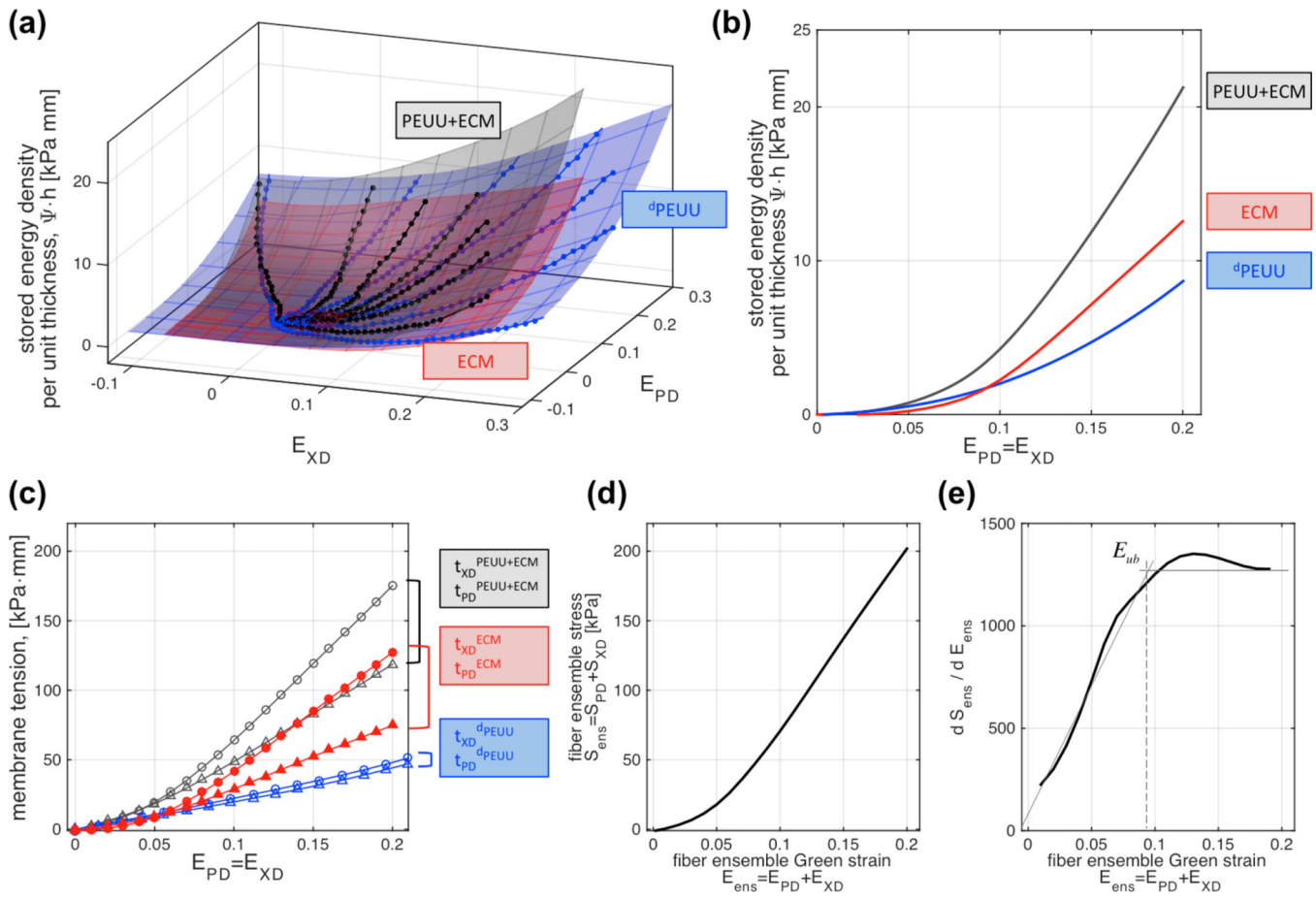

Figure 8.

Evaluation of the mechanical response of the de novo ECM: A) seven protocol biaxial test data before (PEUU+ECM, blue dots) and after (^{d}PEUU black dots) degradation of one representative sample (30% strain, 21 days), and fitted ψ-surfaces of construct, scaffold, and de novo ECM (blue, red and green respectively); B) stored energy density under equi-strain conditions; C) membrane tension response under equi-strain conditions, D) fiber ensemble stress vs. strain response; and E) rate of change of ensemble stress vs. ensemble strain (recruitment).

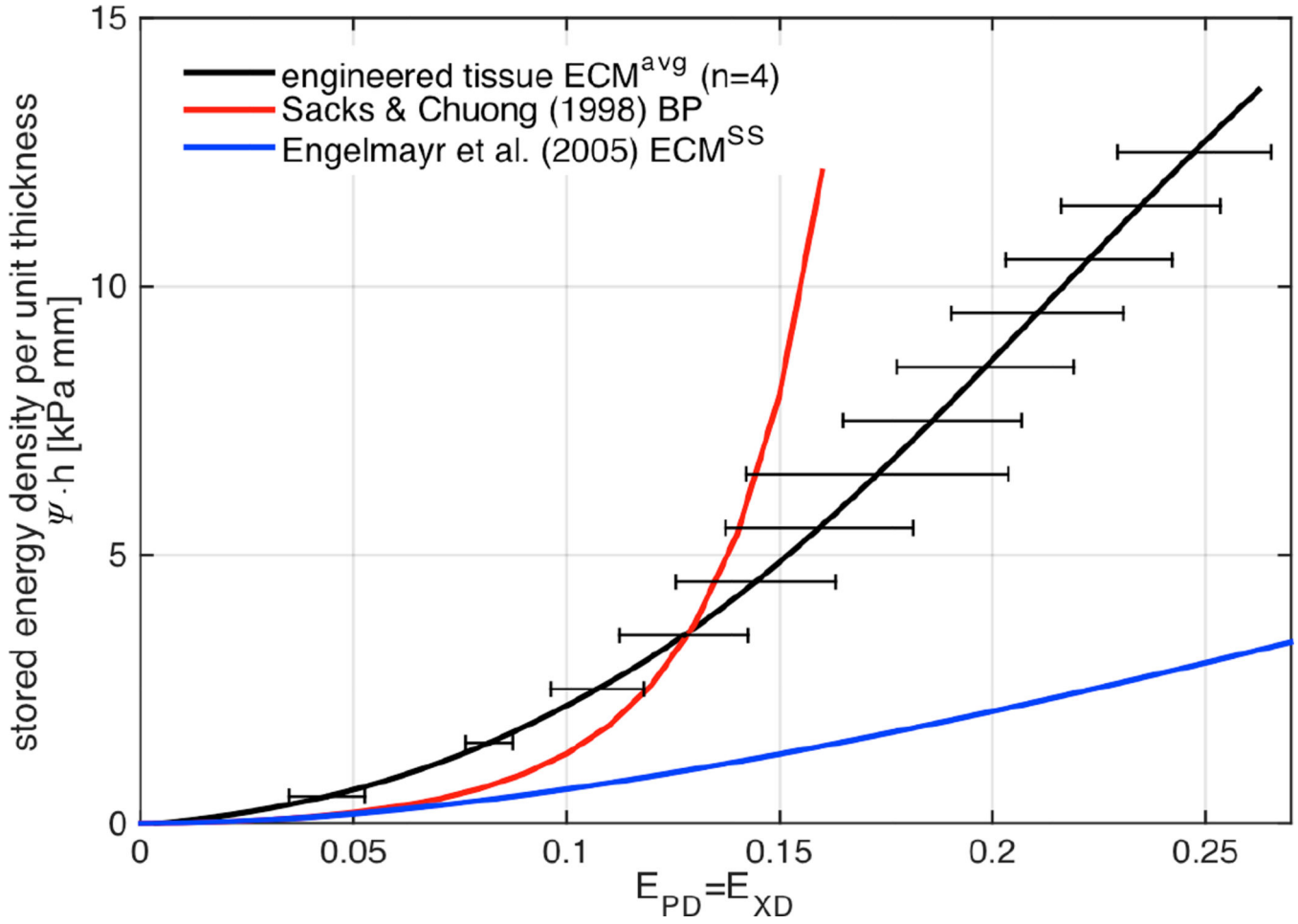

Figure 9.

Stored energy density under equi-strain conditions of the response of the average engineered tissue de novo ECM (21 days, 30% strain, n = 4, black), bovine pericardium (red), and previously obtained engineered tissue with small strain conditioning.

Table 1

Matrix area quantification.

			% area fraction			Area fraction (sq. μm)		
Specimen	**Treatment**	**Stain**	**PEUU**	**ECM**	**Void**	**PEUU**	**ECM**	**Void**
1			75.7	15.4	8.9	204.4	41.6	24.0
2			69.2	18.2	12.6	214.5	56.4	39.1
3	14 day 30% strain	PSR	77.8	15.9	6.3	241.2	49.3	19.5
4			78.2	9.3	12.5	242.4	28.8	38.8
5			74.3	16.4	9.3	230.3	50.8	28.8
		Mean	75.0	15.0	9.9	226.6	45.4	30.0
		SEM	1.6	1.5	1.2	7.5	4.8	3.9

			% area fraction			Area fraction (sq. μm)		
Specimen	**Treatment**	**Stain**	**PEUU**	**ECM**	**Void**	**PEUU**	**ECM**	**Void**
1			57.0	13.9	29.1	245.1	59.8	125.1
2			63.2	10.4	26.4	177.0	29.1	73.9
3	21 day 30% strain	H&E	58.9	14.4	26.7	164.9	40.3	74.8
4			55.2	18.9	25.9	154.6	52.9	72.5
5			60.2	12.5	27.3	168.6	35.0	76.4
		Mean	58.9	14.0	27.1	182.0	43.4	84.5
		SEM	1.4	1.4	0.6	16.2	5.7	10.2

Table 2

Structural model coefficients and physical parameters

Specimen	η [kPa]	μ [deg]	σ [deg]	μ_R	σ_R	E_{ub}	R^2
1	7570.19	131.95	40.68	0.000785	0.000519	0.00241	0.874
2	8095.66	142.44	39.82	0.000264	0.000265	0.000817	0.977
4	11427.05	129.55	41.6	0.0000505	0.0005141	0.000251	0.984
5	9626.34	143.70	5.73	0.0412	0.0393	0.1044	0.921
avg ± std	9179.91 ± 1501.31	136.91 ± 6.23	31.96 ± 15.16	0.0106 ± 0.0118	0.0101 ± 0.0168	0.0270 ± 0.0448	
ET ECM^{avg}	9936.93	120.66	34.78	0.000114	0.000113	0.000366	0.989
S&C1998 BP	21001.91	−0.19	37.99	0.2169	0.0295	0.25	0.999